Lithos 142-143 (2012) 267–284

Contents lists available at SciVerse ScienceDirect

Lithos

journal homepage: www.elsevier.com/locate/lithos

Diamonds and their mineral inclusions from the Renard kimberlites in Quebec

Lucy Hunt [a,*], Thomas Stachel [a], Tom E. McCandless [a,b], John Armstrong [c], Karlis Muelenbachs [a]

[a] Department of Earth and Atmospheric Sciences, University of Alberta, Edmonton, AB, Canada, T6G 2E3
[b] MCC Geoscience, Incorporated, 1925 Fell Avenue, North Vancouver, British Columbia, Canada, V7P 3G6
[c] Stornoway Diamond Corporation, Unit 116-980 West 1st Street, North Vancouver, B.C, Canada, V7P 3N4

ARTICLE INFO

Article history:
Received 16 September 2011
Accepted 25 February 2012
Available online 10 March 2012

Keywords:
Diamond
Carbonation
Coesite
Carbon isotopes
Nitrogen
Superior Craton

ABSTRACT

Mineral inclusions in diamonds from the Renard kimberlites, on the eastern Superior Craton, document an almost exclusively peridotitic inclusion suite with an unusually high abundance of SiO_2 phases (coesite and presumably retrograde quartz). Whilst coesite is often associated with eclogitic diamond sources, there is an almost complete absence of unequivocally eclogitic mineral inclusions at Renard. Consequently, the presence of abundant SiO_2 inclusion phases is likely caused by influx of CO_2 within localised regions of the lithospheric mantle with very high fluid/rock ratios. This caused a progression of carbonation reactions within the host peridotite, likely along veins, locally consuming all olivine, orthopyroxene, and clinopyroxene present and producing free SiO_2.

Nitrogen contents and aggregation states of the diamonds indicate normal mantle residence temperatures, predominantly between 1100 and 1200 °C. Co-variations of carbon isotopic composition and nitrogen content suggest formation from both reducing (CH_4) and oxidising (CO_3^{2-} or CO_2 bearing) melts/fluids. The observation of single diamonds with non-isothermal co-variations of nitrogen content and aggregation state, or containing disequilibrium inclusion parageneses (e.g., variations in olivine Mg# up to 0.5 within single diamonds), indicates that Renard diamonds grew during a number of precipitation events within a physically and chemically changing environment.

1. Introduction

The Superior Craton of Eastern Canada is the largest known contiguous region of Archean crust in the world. Whilst the crustal evolution is well understood (e.g. Card, 1990 and references therein), little is known about the underlying sub-continental lithospheric mantle (SCLM). Mantle derived xenoliths and xenocrysts provide information on the formation and history of the lithospheric mantle, but may not be representative of the SCLM at the time of diamond formation, due to a complex subsequent history (Griffin et al., 1999; Stachel et al., 1998b). The study of diamonds and their mineral inclusions provides an alternative means of directly sampling the Earth's upper mantle. During the growth of diamonds, syngenetic mineral inclusions can be trapped and enclosed (Harris, 1968). Diamonds are chemically inert and inclusions are protected from chemical alteration, thus preserving their original mantle signature during their mantle residence and transport to the surface. Inclusions, therefore, provide the only pristine information on the cratonic mantle at the time of diamond formation.

Our study of diamonds from the Renard kimberlites complements previous work on mantle xenoliths/xenocrysts and diamonds from the Superior Craton (e.g. Armstrong et al., 2004; Griffin et al., 2004; Hunt, 2011; Sage et al., 1996; Scully, 2000; Scully et al., 2004; Stachel et al., 2006; Van Rythoven et al., 2011) and provides new information on the SCLM. A comprehensive study on the carbon isotopic composition of the diamonds was performed to identify possible diamond forming agents. Inclusion and nitrogen based thermometry was used to constrain the physical conditions of diamond formation and mantle residence. Finally, the composition of syngenetic and epigenetic mineral inclusions provides information on the composition and evolution of the SCLM during and after diamond growth, respectively.

2. Geological background

The Renard bodies are located within a 2 km^2 area in the northern Otish Mountains of Quebec (Fig. 1), 820 km north of Montreal. Ashton Mining of Canada (now Stornoway Diamond Corporation) and its joint venture partner Soquem Inc. discovered the pipes in 2001. The initial discovery identified 10 kimberlite pipes. Later work determined that Renards 5 and 6 joined at depth, and consequently the name Renard 65 was introduced. Of these nine pipes, four are of particular economic interest due to high initial diamond grades: Renards 2, 3, 4 and 9.

The Renard kimberlites classify as Group I (Birkett et al., 2004; Fitzgerald et al., 2008) and are part of the Otish kimberlitic volcanic event. Emplacement has been dated to the Neoproterozoic

* Corresponding author. Tel.: +1 780 492 3265; fax: +1 780 492 2030.
E-mail address: lchunt@ualberta.ca (L. Hunt).

0024-4937/$ – see front matter © 2012 Elsevier B.V. All rights reserved.
doi:10.1016/j.lithos.2012.02.022

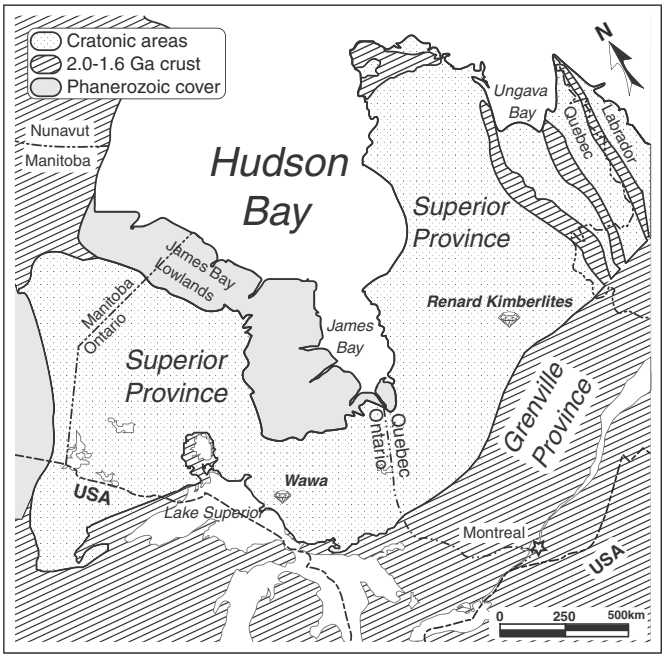

Fig. 1. Simplified geological map of the Superior Province and adjacent areas showing the location of the Renard Kimberlites (redrawn using information from: Hoffman, 1988; Card, 1990).

(631.6 +/− 3.5 Ma Birkett et al., 2004: 640.5 +/− 2.8 Ma Fitzgerald et al., 2008). This is broadly coeval with the conversion from subduction magmatism to rifting in northern Laurentia (Birkett et al., 2004). The kimberlites are emplaced into Archean granitic and gneissic host rocks of the Opinaca Subprovince (Percival, 2007). Xenoliths and xenocrysts from the kimberlites also indicate a late Archean age for the formation of the SCLM beneath Renard (Hunt, 2011).

3. Samples

Our study is based on a subset of 56 diamonds, strongly biased toward inclusion bearing samples, recovered during mini-bulk sampling of five of the nine Renard kimberlite pipes: Four diamonds are from Renard 1; 15 from Renard 2; eight from Renard 3; 17 from Renard 4; and 12 from Renard 65. The diamonds were selected from +0.85 mm to +3.35 mm square mesh sieve size fractions, ranging in weight from 1.5 mg to 152.8 mg (0.008–0.764 carats) (Appendix A1).

All the diamonds were visually studied and classified based on their physical characteristics. Inclusions were recovered from 33 of the diamonds and analysed by electron microprobe. All diamonds were analysed for their carbon isotopic composition and their nitrogen content and aggregation state.

4. Analytical techniques

4.1. Inclusions

Inclusions were identified, where possible, with the aid of a stereomicroscope, prior to diamond breakage. At this time, the inclusions were evaluated for possible alteration through fractures connecting to the diamond surface. Mineral inclusions were then released from the diamonds using a steel breaker. The recovered inclusions were mounted in brass pips using Araldite® epoxy resin and polished on a wheel with increasingly finer polishing media finishing with 0.05 μm alumina suspension.

The major and minor element compositions of the inclusions were measured by wavelength-dispersive spectrometry (WDS) on a JEOL JXA-8900 Superprobe at the University of Alberta. Silicate, oxide and metal standards were used and analyses were conducted with an accelerating voltage of 20 kV and a beam current of 20 nA. Peak count times for each element were 30–60 s with half the time on each background. Where possible, three spots were measured on each sample and averaged, in cases where the grains were determined to be homogeneous. For averaged analyses, detection limits are ≤0.01 wt.% for all oxides with the exception of Na_2O (≤0.02 wt.%) and P_2O_5 (≤0.03 wt.%).

$Mg\#_{Ca\text{-}corr.}$ ($Mg\#_{Ca\text{-}corr.} = Mg\# + 2Ca$: Ca as cations calculated on a basis of 24 oxygens, following Stachel et al., 2003) is given for garnet inclusions to account for the effect of CaO on Mg/Fe partitioning between garnet and Mg–Fe silicates (O'Neill and Wood, 1979).

For SiO_2 phase inclusions Raman Spectroscopy was performed to determine the crystal structure. A Nicolet Almega XR Dispersive Raman spectrometer was used with a 5.32 nm and 24 mW laser at the National Institute for Nanotechnology at the University of Alberta.

4.2. Nitrogen content and aggregation state

The concentration and aggregation state of nitrogen impurities within the diamonds was determined by FTIR spectroscopy using a Thermo-Nicolet Nexus 470 FTIR spectrometer coupled with a Nicolet Continuum infrared microscope. The spectra were collected for 200 s in transmittance mode for a range in wave number from 650 to 4000 cm^{-1}. The spectral resolution is 4 cm^{-1} and an aperture of 100 μm was used.

A Type II diamond standard was analysed, baseline corrected and converted to absorption coefficient (absorbance of a 1 cm thick sample) through normalisation of the absorbance at 1995 cm^{-1} to 11.94 cm^{-1}. The sample spectra were first baselined and then, through a combined subtraction and normalization procedure involving the Type II diamond spectrum, converted to absorption coefficient. Sample spectra were deconvoluted into the A, B and D components based on software provided by David Fisher (Research Laboratories of the Diamond Trading Company, Maidenhead, UK). Concentrations of nitrogen (atomic ppm) were calculated using absorption coefficient values at 1282 cm^{-1} for the A- (Boyd et al., 1994: 16.5 ± 1) and B-centre (Boyd et al., 1995: 79.4 ± 8).

Analyses were performed on diamond fragments breakage for inclusion recovery. Multiple analyses on each diamond were completed in order to detect variations in nitrogen content and aggregation state within individual stones. The detection limits depend strongly on the quality of the fragments, but are generally in the range 5–15 at. ppm, with relative errors for concentration and aggregation state for each measurement being at the level of ~5–10%.

4.3. Carbon isotopic composition

The carbon isotopic composition of the diamonds was determined using a Finnigan MAT 252 gas flow mass spectrometer at the University of Alberta. Inclusion and graphite free diamond fragments (0.3–2 mg) were combusted at 980 °C in sealed and evacuated quartz tubes for ~12 h with 1.0–2.0 g of CuO as an oxygen source. The results are reported relative to the V-PDB standard (Coplen et al., 1983). Instrumental precision is in the order of +/− 0.02‰.

5. Results

5.1. Diamond characteristics

5.1.1. Morphology

The morphologies of the 56 diamonds include primary octahedra (12%) and resorbed rounded dodecahedral shapes (50%; see Appendix A1). The occurrence of pseudohemimorphic morphologies (4%) indicates that some diamonds protruded from their host xenoliths/xenocrysts during kimberlite ascent, causing differential resorption. Diamonds showing a herringbone line, defining the compositional

plane of a twin, are identified as macles (18%). Samples comprising irregular intergrowth of two or more stones are classified as aggregates (16%). Diamond fragments and other types of irregular stones are categorised according to their residual features.

In the same size range, an unbiased selection (not chosen for inclusion content) of 97 unbroken stones from Renard 2, classified by Stornoway Diamond Corp. consisted of 7% octahedra, 45% dodecahedra, 7% twins and 41% aggregates (McCandless pers. comms).

5.1.2. Colour

The examined Renard diamonds are colourless or exhibit either yellow or brown to pink-brown colouration of varying intensity. Yellow colouration is produced by nitrogen impurities giving rise to N3 and N2 centres within diamond (Collins, 1982). Brown and pink colouration is caused by plastic deformation and is attributed to the formation of defects in the diamond lattice due to strain (Harris, 1987).

The majority of the diamonds have a pale/very pale yellow (38%) or a pale/very pale brown colour (23%). A further 2% have a stronger yellow colour, 9% have a more intense brown colour and 2% have a pink brown colour. The remaining 27% of the diamonds are colourless (Appendix A1). No correlation is observed between morphology and colour.

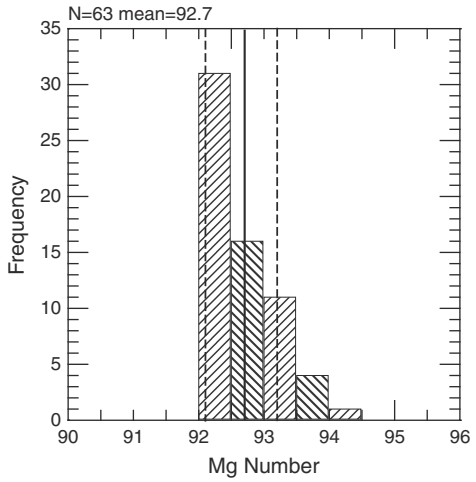

Fig. 2. Mg# of Renard olivine inclusion. Solid line represents mean (92.7). Dashed lines represent mean compositions of lherzolitic (92.1) and harzburgitic (93.2) olivine inclusions worldwide (Stachel and Harris, 2008). Xenolithic harzburgitic olivine from Renard also shows a mean Mg# of 93.2 (Hunt, 2011).

5.1.3. Surface features

The surface features observed on the 56 diamonds relate to the morphology of the diamond, with specific features associated with dodecahedral faces, and others seen only on octahedral faces (e.g. Robinson, 1979). Due to the predominance of dodecahedral diamonds, surface features related to resorption of primary octahedral growth layers are dominant.

Terracing and hillocks on dodecahedral faces are the most abundant surface features – observed on 36% and 50% of the diamonds respectively. Trigons are present on all octahedra and are common (45%) on residual octahedral faces. Plastic deformation lines are observed on 46% of the diamonds and are commonly associated with brown colouration. Other surface features observed include: stacked growth layers; tetragons on etched {100} fracture faces; and, observed in only one case, a microdisk pattern (Appendix A1).

Dark green spots were recognised on 23% of the samples and are particularly abundant in pipes 65, where 75% ($n=9$) of the stones have one or more green spots. These spots result from defects in the diamond lattice caused by alpha particle irradiation, and indicate prolonged contact with radioactive minerals (Harris, 1987; Meyer et al., 1965).

One diamond (also from pipe 65) exhibits elongate green depressions on its faces (Appendix C1). The outside of the diamond is irregular, possibly representing a partially resorbed coat. The depressions are interpreted as voids left by mineral inclusions within the diamond coat that have subsequently been removed. The green colouration is interpreted as resulting from the same processes (alpha particle irradiation resulting from radioactive decay in the inclusion minerals) that generates green spots on diamond surfaces.

5.2. Inclusions in diamond

5.2.1. Syngenetic inclusions

5.2.1.1. Olivine. Olivine is the dominant mineral inclusion within the Renard suite. Sixty-three olivine inclusions were recovered from 16 diamonds. The olivines have Mg-numbers (Mg#) ranging from 92.1 to 94.3 with a mean of 92.7 (Fig. 2, Table 1). The forsterite content varies (ΔFo) up to 0.5 among multiple inclusions within single diamonds (e.g., diamond 12036b: ΔFo 0.37; 13547b: ΔFo 0.45; 13805a: ΔFo 0.45). The mean is between the worldwide mean of lherzolitic and harzburgitic diamond inclusion olivines (92.1 and 93.2, respectively), and coincides with the mean of samples of unknown, likely mixed, parageneses (Fig. 2) (Stachel and Harris, 2008). This is confirmed statistically with a student *t*-test, by comparing the olivine inclusions with all three groupings in the database of Stachel and Harris (2008). The test indicated that, with 99% confidence, the Renard olivine inclusions are not either purely harzburgitic nor lherzolitic populations but are indistinguishable from the worldwide data set for olivine inclusions of unknown (and mixed) paragenesis. The range in forsterite content for olivine inclusions does, however, encompass the composition of harzburgitic olivines in microxenoliths from the Renard kimberlites (92.7–93.5, mean 93.2: Hunt, 2011).

Two olivines from one diamond (13539a) have CaO contents of 0.05 wt.% indicating a high likelihood that they crystallised in equilibrium with clinopyroxene. The remainder all have CaO contents ≤0.04 wt.% CaO, which may be suggestive of a harzburgitic paragenesis. However, precipitation of lherzolitic olivine along a "cool" geothermal gradient and in the uppermost part of the diamond stability field could equally explain CaO contents as low as 0.01 wt.% (Stachel and Harris, 2008).

5.2.1.2. Orthopyroxene. Five orthopyroxenes were recovered from three diamonds. All have Al_2O_3 contents ranging from 0.4–0.7 wt.%, and CaO contents from 0.1–0.8 wt.%. Two orthopyroxenes from diamond 13521c have Mg# of 94.6, two orthopyroxenes from diamond 13538 have Mg# of 93.6, and the orthopyroxene from diamond 13532a has an Mg# of 93.0 (Table 1). Using the CaO vs. Mg# discrimination diagram of Stachel and Harris (2008) orthopyroxenes from diamonds 13538 and 13532a plot within the region occupied by both harzburgitic and lherzolitic inclusions. The inclusions from stone 13521c, however, lie in the compositional space for harzburgitic inclusions only. This agrees with orthopyroxenes in microxenoliths from the Renard kimberlites, which have Mg# from 93.2 to 94.3 (mean 93.8) for the harzburgitic paragenesis and Mg# from 88.1 to 93.8 (mean 92.6) for the lherzolitic paragenesis (Hunt, 2011).

5.2.1.3. Garnet. Two garnet inclusions were recovered from two stones: 12013 and 13523. The garnets are chrome pyropes, with concentrations of 3.1 and 3.8 wt.% CaO, 8.7 and 10.2 wt.% Cr_2O_3, 23.2 and 22.3 wt.% MgO and 6.3 and 5.9 wt.% FeO, respectively. Compositionally the garnets classify as type G10D in the classification scheme of Grütter et al. (2004), i.e. they derive from diamond facies harzburgitic sources. The $Mg\#_{Ca\_corr}$ of the two garnets are 87.7 and 88.3 respectively (Table 1), falling within the range for harzburgitic garnet

Table 1
Table of the syngenetic inclusion electron microprobe data. Atoms per formula unit calculated assuming stoichiometry on the basis of ideal atoms of oxygens. Olv. – olivine, gnt – garnet, SiO_2 – coesite, chr. – chromite, cpx – clinopyroxene, opx – orthopyroxene, pyr. – pyrrhotite, p – peridotite, p(H) – harzburgite, p(L) – lherzolite, e – eclogite, ? – unknown paragenesis.

Diamond	12001		12013			12014		12016a	12018	12031				12036a			
Inclusion	-1	-2	-1	-2	-6	-2	-4	-3	-3	-2	-3	-113	-111	-2	-6	-8	-12
Mineral	Olv	Olv	Gnt	Olv	Olv	SiO_2	SiO_2	Olv	SiO_2	Chr	Chr	Chr	Chr	Olv	SiO_2	SiO_2	Olv
Paragen.	p	p	p(H)	p(H)	p(H)	?	?	p	?	p	p	p	p	p	p	p	p
Assem.	olv	olv	olv, gnt	olv, gnt	olv, gnt	SiO_2	SiO_2	olv	SiO_2	chr	chr	chr	chr	olv,SiO_2	olv,SiO_2	olv,SiO_2	olv,SiO_2
SiO_2	40.29	41.31	41.17	40.61	40.38	101.56	101.24	40.23	100.38	0.24	0.18	0.26	0.23	40.49	98.25	101.18	40.78
TiO_2	≤0.00	≤0.00	0.03	≤0.00	≤0.00	≤0.00	≤0.00	≤0.00	≤0.00	0.03	0.03	0.02	0.04	0.01	0.16	≤0.00	≤0.00
Al_2O_3	≤0.00	0.01	16.57	0.03	0.03	0.02	0.04	0.01	0.19	7.27	7.72	7.70	7.55	0.01	1.42	0.03	0.02
Cr_2O_3	0.03	0.07	8.68	0.07	0.07	≤0.00	≤0.00	0.05	≤0.00	63.52	63.56	65.30	64.51	0.06	≤0.00	≤0.00	0.06
FeO	7.55	7.74	6.34	7.41	7.33	1.13	1.20	7.77	0.01	13.72	14.01	14.14	14.02	7.10	0.11	0.01	7.28
NiO	0.34	0.36	0.01	0.33	0.33	≤0.00	≤0.00	0.35	≤0.00	0.10	0.09	0.11	0.10	0.35	0.01	≤0.00	0.35
MnO	0.11	0.12	0.35	0.14	0.14	0.03	0.03	0.12	≤0.00	0.39	0.41	0.38	0.36	0.11	0.01	0.01	0.11
MgO	50.55	50.40	23.21	51.47	52.20	≤0.00	0.01	53.09	0.01	14.82	14.67	14.97	15.20	50.41	0.11	≤0.00	50.71
CaO	0.02	0.04	3.06	0.03	0.03	0.01	≤0.00	0.03	≤0.00	≤0.00	≤0.00	≤0.00	≤0.00	0.03	0.05	≤0.00	0.03
Na_2O	0.02	0.01	0.01	0.01	0.01	0.01	0.01	0.01	0.02	0.02	0.02	0.01	0.01	0.02	0.05	0.02	0.02
K_2O	≤0.00	≤0.00	≤0.00	≤0.00	≤0.00	≤0.00	≤0.00	≤0.00	≤0.00	≤0.00	≤0.00	≤0.00	≤0.00	≤0.00	0.31	≤0.00	≤0.00
Total	98.93	100.05	99.46	100.10	100.53	102.75	102.54	101.68	100.62	100.31	100.93	103.13	102.24	98.58	100.47	101.24	99.37
Si	0.99	1.00	2.99	0.99	0.98	1.00	0.99	0.97	1.00	0.01	0.01	0.01	0.01	1.00	0.98	1.00	1.00
Ti	≤0.00	≤0.00	≤0.00	≤0.00	≤0.00	≤0.00	≤0.00	≤0.00	≤0.00	≤0.00	≤0.00	≤0.00	≤0.00	≤0.00	≤0.00	≤0.00	≤0.00
Al	≤0.00	≤0.00	1.42	≤0.00	≤0.00	≤0.00	≤0.00	≤0.00	≤0.00	0.28	0.29	0.29	0.28	≤0.00	0.02	≤0.00	≤0.00
Cr	≤0.00	≤0.00	0.50	≤0.00	≤0.00	≤0.00	≤0.00	≤0.00	≤0.00	1.63	1.62	1.63	1.63	≤0.00	≤0.00	≤0.00	≤0.00
Fe2 +	0.16	0.16	0.38	0.15	0.15	0.01	0.01	0.16	≤0.00	0.37	0.38	0.37	0.37	0.15	≤0.00	≤0.00	0.15
Ni	0.01	0.01	≤0.00	0.01	0.01	≤0.00	≤0.00	0.01	≤0.00	≤0.00	≤0.00	≤0.00	≤0.00	0.01	≤0.00	≤0.00	0.01
Mn	≤0.00	≤0.00	0.02	≤0.00	≤0.00	≤0.00	≤0.00	≤0.00	≤0.00	0.01	0.01	0.01	0.01	≤0.00	≤0.00	≤0.00	≤0.00
Mg	1.85	1.82	2.51	1.86	1.88	≤0.00	≤0.00	1.90	≤0.00	0.72	0.71	0.71	0.72	1.85	≤0.00	≤0.00	1.85
Ca	≤0.00	≤0.00	0.24	≤0.00	≤0.00	≤0.00	≤0.00	≤0.00	≤0.00	≤0.00	≤0.00	0.00	≤0.00	≤0.00	≤0.00	≤0.00	≤0.00
Na	≤0.00	≤0.00	≤0.00	≤0.00	≤0.00	≤0.00	≤0.00	≤0.00	≤0.00	≤0.00	≤0.00	≤0.00	≤0.00	≤0.00	≤0.00	≤0.00	≤0.00
K	≤0.00	≤0.00	≤0.00	≤0.00	≤0.00	≤0.00	≤0.00	≤0.00	≤0.00	≤0.00	≤0.00	≤0.00	≤0.00	≤0.00	≤0.00	≤0.00	≤0.00
Total	3.01	3.00	8.06	3.01	3.02	1.00	1.01	3.03	1.00	3.03	3.03	3.03	3.03	3.00	1.01	1.00	3.00
Oxygens	4.00	4.00	12.00	4.00	4.00	2.00	2.00	4.00	2.00	4.00	4.00	4.00	4.00	4.00	2.00	2.00	4.00
Mg#	92.27	92.07	86.71	92.53	92.69			92.42		65.83	65.12	65.35	65.89	92.68			92.55

Diamond	12036a		12036b									12035b		12041			
Inclusion	-19	-20	-1	-3	-4	-6	-7	-114	-116	-117	-121	-115	-118	-1	-2	-3a	-5
Mineral	Olv	SiO_2	Olv	Olv	SiO_2	Olv	Olv	Olv	Olv	Olv	SiO_2	Olv	Olv	Olv	Olv	Olv	Olv
Paragen.	p	p	p	p	p	p	p	p	p	p	p	p	p	p	p	p	p
Assem.	olv, SiO_2	olv, SiO_2	olv, SiO_2	olv, SiO_2	olv, SiO_2	olv, SiO_2	olv, SiO_2	olv, SiO_2	olv, SiO_2	olv, SiO_2	olv	olv	olv	olv	olv	olv	olv
SiO_2	40.24	99.10	41.10	40.63	100.32	40.19	40.91	40.03	38.71	40.08	100.59	39.97	41.82	40.58	40.08	40.37	41.32
TiO_2	≤0.00	0.01	≤0.00	0.01	≤0.00	≤0.00	≤0.00	≤0.00	≤0.00	0.01	≤0.00	≤0.00	0.01	≤0.00	≤0.00	≤0.00	≤0.00
Al_2O_3	0.03	0.01	0.01	0.02	0.02	0.27	0.10	0.40	0.02	0.01	0.01	0.05	0.02	0.02	0.05	0.02	0.04
Cr_2O_3	0.06	≤0.00	0.06	0.06	≤0.00	0.05	0.06	0.04	0.05	0.06	0.01	0.06	0.06	0.07	0.06	0.06	0.06
FeO	7.25	0.01	7.26	7.15	1.07	7.54	7.05	7.16	7.25	7.35	≤0.00	7.24	7.31	7.59	7.60	7.66	7.43
NiO	0.35	≤0.00	0.34	0.35	≤0.00	0.34	0.35	0.33	0.32	0.36	≤0.00	0.34	0.33	0.36	0.37	0.36	0.36
MnO	0.10	0.01	0.11	0.10	0.01	0.16	0.10	0.10	0.10	0.13	0.01	0.11	0.11	0.11	0.11	0.10	0.11
MgO	49.92	≤0.00	50.90	50.50	≤0.00	51.17	50.90	50.41	53.24	51.58	0.01	51.86	50.57	51.23	50.89	50.72	50.07
CaO	0.03	≤0.00	0.03	0.03	≤0.00	0.03	0.04	0.03	0.04	0.03	0.01	0.04	0.03	0.04	0.04	0.03	0.04
Na_2O	0.02	≤0.00	0.01	0.02	≤0.00	0.01	0.02	0.02	0.02	0.01	≤0.00	0.02	0.02	0.03	0.01	0.01	0.03
K_2O	≤0.00	≤0.00	≤0.00	≤0.00	≤0.00	≤0.00	≤0.00	≤0.00	≤0.00	≤0.00	≤0.00	≤0.00	≤0.00	≤0.00	≤0.00	≤0.00	≤0.00
Total	98.01	99.12	99.84	98.86	101.43	99.77	99.55	98.51	99.76	99.61	100.62	99.69	100.29	100.03	99.24	99.34	99.45
Si	1.00	1.00	1.00	1.00	1.00	0.98	1.00	0.99	0.95	0.98	1.00	0.98	1.01	0.99	0.98	0.99	1.01
Ti	≤0.00	≤0.00	≤0.00	≤0.00	≤0.00	≤0.00	≤0.00	≤0.00	≤0.00	≤0.00	≤0.00	≤0.00	≤0.00	≤0.00	≤0.00	≤0.00	≤0.00
Al	≤0.00	≤0.00	≤0.00	≤0.00	≤0.00	0.01	≤0.00	0.01	≤0.00	≤0.00	≤0.00	≤0.00	≤0.00	≤0.00	≤0.00	≤0.00	≤0.00
Cr	≤0.00	≤0.00	≤0.00	≤0.00	≤0.00	≤0.00	≤0.00	≤0.00	≤0.00	≤0.00	≤0.00	≤0.00	≤0.00	≤0.00	≤0.00	≤0.00	≤0.00
Fe2 +	0.15	≤0.00	0.15	0.15	0.01	0.15	0.14	0.15	0.15	0.15	≤0.00	0.15	0.15	0.15	0.16	0.16	0.15
Ni	0.01	≤0.00	0.01	0.01	≤0.00	0.01	0.01	0.01	0.01	0.01	≤0.00	0.01	0.01	0.01	0.01	0.01	0.01
Mn	≤0.00	≤0.00	≤0.00	≤0.00	≤0.00	≤0.00	0.00	≤0.00	≤0.00	≤0.00	≤0.00	≤0.00	≤0.00	≤0.00	≤0.00	≤0.00	≤0.00
Mg	1.84	≤0.00	1.84	1.85	0.00	1.86	1.85	1.85	1.94	1.88	≤0.00	1.89	1.82	1.86	1.86	1.85	1.82
Ca	≤0.00	≤0.00	≤0.00	≤0.00	≤0.00	≤0.00	≤0.00	≤0.00	≤0.00	≤0.00	≤0.00	≤0.00	≤0.00	≤0.00	≤0.00	≤0.00	≤0.00
Na	≤0.00	≤0.00	≤0.00	≤0.00	≤0.00	≤0.00	≤0.00	≤0.00	≤0.00	≤0.00	≤0.00	≤0.00	≤0.00	≤0.00	≤0.00	≤0.00	≤0.00
K	≤0.00	≤0.00	≤0.00	≤0.00	≤0.00	≤0.00	≤0.00	≤0.00	≤0.00	≤0.00	≤0.00	≤0.00	≤0.00	≤0.00	≤0.00	≤0.00	≤0.00
Total	3.00	1.00	3.00	3.00	1.00	3.02	3.00	3.01	3.05	3.02	1.00	3.02	2.99	3.01	3.02	3.01	2.99
Oxygens	4.00	2.00	4.00	4.00	2.00	4.00	4.00	4.00	4.00	4.00	2.00	4.00	4.00	4.00	4.00	4.00	4.00
Mg#	92.47		92.59	92.64		92.36	92.79	92.62	92.90	92.60		92.74	92.50	92.33	92.27	92.19	92.32

Diamond	12041	13520	13521b-1	13521c-1			13523			13530a		13530b				13530c	
Inclusion	-6	-9	-1	-1	-3	-4	-6	-7	-8	-110	-110b	-113	-114	-115	-115a	-1	-2
Mineral	Olv	Chr	SiO_2	Opx	SiO2	Opx	Olv	Olv	Garnet	Olv	Chr	Olv	Olv	Olv	Chr	Chr	Chr
Paragen.	p	p	?	p	p	p	p(H)	p(H)	p(H)	p	p	p	p	p	p	p	p
Assem.	olv	chr	SiO_2	opx, SiO_2	opx, SiO_2	opx, SiO_2	olv, gnt	olv, gnt	olv, gnt	olv, chr	olv, chr	olv, chr	olv, chr	olv, chr	olv, chr	chr	chr
SiO_2	38.72	0.22	100.89	58.12	96.22	57.44	41.09	41.18	41.66	41.24	0.10	40.92	41.04	41.06	0.21	0.20	0.22
TiO_2	≤0.00	0.04	≤0.00	0.01	≤0.00	0.01	≤0.00	≤0.00	0.06	0.01	0.13	0.01	≤0.00	0.01	0.13	0.13	0.12
Al_2O_3	0.01	6.50	0.01	0.72	0.02	0.71	0.02	0.05	16.11	0.01	7.90	0.01	0.17	0.05	7.49	7.87	7.98
Cr_2O_3	0.06	65.28	≤0.00	0.51	≤0.00	0.54	0.04	0.05	10.15	0.06	65.73	0.10	0.09	0.09	65.64	64.64	63.74
FeO	7.64	14.12	≤0.00	3.68	≤0.00	3.73	7.11	7.03	5.87	5.65	13.39	6.03	6.17	6.09	12.66	12.21	12.14
NiO	0.34	0.09	0.01	0.11	≤0.00	0.11	0.35	0.35	0.01	0.34	0.07	0.31	0.31	0.32	0.09	0.10	0.09
MnO	0.12	0.37	0.01	0.10	0.01	0.10	0.09	0.11	0.31	0.08	0.37	0.08	0.08	0.09	0.36	0.36	0.35
MgO	50.78	14.53	≤0.00	36.16	0.01	36.56	50.93	50.59	22.27	52.41	14.44	51.61	51.43	51.92	14.81	15.71	15.82
CaO	0.03	≤0.00	0.01	0.11	≤0.00	0.12	0.02	0.02	3.81	0.02	≤0.00	0.02	0.02	0.02	≤0.00	0.01	≤0.00
Na_2O	0.01	0.02	0.01	0.04	0.01	0.03	0.02	0.02	0.03	0.02	0.03	0.02	0.02	0.02	0.02	0.02	0.01
K_2O	≤0.00	≤0.00	≤0.00	≤0.00	≤0.00	≤0.00	0.01	0.01	≤0.00	≤0.00	≤0.00	≤0.00	≤0.00	≤0.00	≤0.00	≤0.00	≤0.00
Total	97.71	101.36	100.94	99.56	96.27	99.36	99.67	99.39	100.32	99.84	102.33	99.13	99.36	99.65	101.58	101.41	100.64
Si	0.97	0.01	1.00	1.99	1.00	1.97	1.00	1.00	3.00	0.99	≤0.00	1.00	1.00	0.99	0.01	0.01	0.01
Ti	≤0.00	≤0.00	≤0.00	≤0.00	≤0.00	≤0.00	≤0.00	≤0.00	≤0.00	≤0.00	≤0.00	≤0.00	≤0.00	≤0.00	≤0.00	≤0.00	≤0.00
Al	≤0.00	0.25	≤0.00	0.03	≤0.00	0.03	≤0.00	≤0.00	1.37	≤0.00	0.30	≤0.00	≤0.00	≤0.00	0.28	0.30	0.30
Cr	≤0.00	1.67	≤0.00	0.01	≤0.00	0.01	≤0.00	≤0.00	0.58	≤0.00	1.65	≤0.00	≤0.00	≤0.00	1.66	1.63	1.62
Fe2+	0.16	0.38	≤0.00	0.11	≤0.00	0.11	0.14	0.14	0.35	0.11	0.36	0.12	0.13	0.12	0.34	0.33	0.33
Ni	0.01	≤0.00	≤0.00	≤0.00	≤0.00	≤0.00	0.01	0.01	0.00	0.01	≤0.00	0.01	0.01	0.01	≤0.00	≤0.00	≤0.00
Mn	≤0.00	0.01	≤0.00	≤0.00	≤0.00	≤0.00	≤0.00	≤0.00	0.02	≤0.00	0.01	≤0.00	≤0.00	≤0.00	0.01	0.01	0.01
Mg	1.89	0.70	≤0.00	1.84	≤0.00	1.87	1.85	1.84	2.39	1.88	0.69	1.87	1.86	1.87	0.71	0.75	0.76
Ca	≤0.00	≤0.00	≤0.00	≤0.00	≤0.00	≤0.00	0.00	0.00	0.29	≤0.00	≤0.00	≤0.00	≤0.00	≤0.00	≤0.00	≤0.00	≤0.00
Na	≤0.00	≤0.00	≤0.00	≤0.00	≤0.00	≤0.00	≤0.00	≤0.00	≤0.00	≤0.00	≤0.00	≤0.00	≤0.00	≤0.00	≤0.00	≤0.00	≤0.00
K	≤0.00	≤0.00	≤0.00	≤0.00	≤0.00	≤0.00	≤0.00	≤0.00	≤0.00	≤0.00	≤0.00	≤0.00	≤0.00	≤0.00	≤0.00	≤0.00	≤0.00
Total	3.03	3.03	1.00	3.99	1.00	4.01	3.00	3.00	8.02	3.00	3.02	3.00	3.00	3.00	3.02	3.03	3.03
Oxygens	4.00	4.00	2.00	6.00	2.00	6.00	4.00	4.00	12.00	4.00	4.00	4.00	4.00	4.00	4.00	4.00	4.00
Mg#	92.22	64.71		94.60		94.59	92.74	92.77	87.12	94.29	65.78	93.85	93.69	93.83	67.58	69.64	69.91

Diamond	13530c								13532a		13533						
Inclusion	3	-3a	-4	-5	-6	-112	-113	-114	-1	-3	-1	-2	-3a	-3b	-3c	-4a	-4b
Mineral	Chr	Chr	Chr	Chr	Chr	Chr	Chr	Chr	Cpx	Opx	Chr	Chr	Chr	Chr	Chr	Chr	Chr
Paragen.	p	p	p	p	p	p	p	p	p(L)	p(L)	p	p	p	p	p	p	p
Assem.	chr	chr	chr	chr	chr	chr	chr	chr	cpx, opx	cpx, opx	chr, olv, SiO_2	chr, olv, SiO_2	chr, olv, SiO_2	chr, olv, SiO_2	chr, olv, SiO_2	chr, olv, SiO_2	chr, olv, SiO_2
SiO_2	0.19	0.23	0.21	0.19	0.22	0.21	0.21	0.20	54.32	58.38	0.21	0.25	0.28	0.21	0.27	0.27	0.28
TiO_2	0.13	0.13	0.14	0.12	0.12	0.14	0.13	0.14	0.16	0.02	0.05	0.06	0.06	0.05	0.05	0.05	0.05
Al_2O_3	7.79	7.61	7.80	7.68	7.76	7.71	7.86	7.71	0.05	0.39	6.76	6.56	6.48	6.50	6.48	6.47	6.60
Cr_2O_3	64.48	64.18	64.62	64.41	64.52	65.77	65.97	65.48	0.19	0.33	65.80	65.35	66.30	66.37	66.37	66.31	65.88
FeO	12.26	12.40	12.24	12.14	12.37	12.66	12.73	12.62	1.63	4.75	14.04	13.97	14.17	14.16	14.16	14.15	14.07
NiO	0.10	0.09	0.10	0.09	0.09	0.09	0.09	0.10	0.01	0.11	0.10	0.10	0.10	0.10	0.10	0.08	0.10
MnO	0.38	0.32	0.37	0.36	0.33	0.34	0.35	0.35	0.07	0.14	0.38	0.35	0.37	0.38	0.37	0.38	0.37
MgO	16.11	15.45	15.84	15.31	15.47	15.68	15.19	15.66	17.07	35.29	14.67	14.91	14.78	14.87	14.58	14.07	14.85
CaO	0.01	0.01	0.01	0.01	≤0.00	≤0.00	0.01	≤0.00	25.09	0.81	0.01	0.01	0.01	0.00	0.01	≤0.00	0.00
Na_2O	≤0.00	0.03	0.02	0.01	≤0.00	0.01	0.01	0.01	0.18	0.14	0.03	0.02	0.01	0.01	0.01	0.03	0.01
K_2O	≤0.00	≤0.00	≤0.00	≤0.00	≤0.00	≤0.00	≤0.00	≤0.00	0.03	≤0.00	≤0.00	≤0.00	≤0.00	0.00	≤0.00	0.00	≤0.00
Total	101.60	100.58	101.52	100.49	101.07	102.78	102.73	102.44	98.80	100.36	102.23	101.76	102.73	102.83	102.59	102.00	102.40
Si	0.01	0.01	0.01	0.01	0.01	0.01	0.01	0.01	2.00	1.99	0.01	0.01	0.01	0.01	0.01	0.01	0.01
Ti	≤0.00	≤0.00	≤0.00	≤0.00	≤0.00	≤0.00	≤0.00	≤0.00	≤0.00	≤0.00	≤0.00	≤0.00	≤0.00	≤0.00	≤0.00	≤0.00	≤0.00
Al	0.29	0.29	0.29	0.29	0.29	0.29	0.29	0.29	≤0.00	0.02	0.26	0.25	0.24	0.24	0.24	0.25	0.25
Cr	1.62	1.63	1.63	1.64	1.63	1.64	1.65	1.64	0.01	0.01	1.67	1.66	1.67	1.67	1.68	1.69	1.67
Fe2+	0.33	0.33	0.33	0.33	0.33	0.33	0.34	0.33	0.05	0.14	0.38	0.38	0.38	0.38	0.38	0.38	0.38
Ni	≤0.00	≤0.00	≤0.00	≤0.00	≤0.00	≤0.00	≤0.00	≤0.00	≤0.00	≤0.00	≤0.00	≤0.00	≤0.00	≤0.00	≤0.00	≤0.00	≤0.00
Mn	0.01	0.01	0.01	0.01	0.01	0.01	0.01	0.01	≤0.00	≤0.00	0.01	0.01	0.01	0.01	0.01	0.01	0.01
Mg	0.76	0.74	0.75	0.74	0.74	0.74	0.72	0.74	0.94	1.80	0.70	0.72	0.70	0.71	0.70	0.68	0.71
Ca	≤0.00	≤0.00	≤0.00	≤0.00	≤0.00	≤0.00	≤0.00	≤0.00	0.99	0.03	≤0.00	≤0.00	≤0.00	≤0.00	≤0.00	≤0.00	≤0.00
Na	≤0.00	≤0.00	≤0.00	≤0.00	≤0.00	≤0.00	≤0.00	≤0.00	0.01	0.01	≤0.00	≤0.00	≤0.00	≤0.00	≤0.00	≤0.00	≤0.00
K	≤0.00	≤0.00	≤0.00	≤0.00	≤0.00	≤0.00	0.00	≤0.00	0.00	≤0.00	≤0.00	≤0.00	≤0.00	0.00	≤0.00	0.00	≤0.00
Total	3.03	3.03	3.03	3.02	3.02	3.02	3.02	3.03	4.00	4.00	3.03	3.03	3.03	3.03	3.03	3.02	3.03
Oxygens	4.00	4.00	4.00	4.00	4.00	4.00	4.00	4.00	6.00	6.00	4.00	4.00	4.00	4.00	4.00	4.00	4.00
Mg#	70.07	68.96	69.75	69.21	69.04	68.82	68.02	68.86	94.93	92.98	65.07	65.55	65.04	65.18	64.73	63.93	65.29

(continued on next page)

Table 1 (*continued*)

Diamond	13533			13537	13538		13539a			13539b		13544	13547b				
Inclusion	-7	-8	-111	-2	-1	-4	-1	-4	-5	-1	-2	-1a	-1	-2	-3	-3	-4
Mineral	SiO_2	SiO_2	Olv	Olv	Opx	Opx	Olv	Olv	Olv	SiO_2	SiO_2	Cpx	Olv	Olv	Olv	Olv	Olv
Paragen.	p	p	p	p	p	p	p	p	p	?	?	p(L)	p	p	p	p	p
Assem.	chr, olv, SiO_2	chr, olv, SiO_2	chr, olv, SiO_2	olv	opx	opx	olv	olv	olv	SiO_2	SiO_2	cpx	olv	olv	olv	olv	olv
SiO_2	102.21	99.78	40.90	41.80	56.79	54.74	41.32	42.70	39.24	99.36	101.89	52.13	40.43	41.22	41.45	41.58	40.83
TiO_2	≤0.00	0.00	0.01	0.01	0.01	0.01	≤0.00	0.01	≤0.00	0.00	0.00	1.62	0.00	≤0.00	0.00	0.00	0.00
Al_2O_3	0.06	0.02	0.02	0.01	0.45	0.50	0.01	0.02	0.01	0.21	0.06	0.86	0.10	0.01	0.00	0.00	0.01
Cr_2O_3	≤0.00	0.01	0.06	0.06	0.30	0.38	0.05	0.05	0.05	0.00	0.00	0.02	0.03	0.07	0.03	0.03	0.07
FeO	0.01	0.00	7.24	7.38	4.46	4.45	7.68	7.54	7.60	1.19	1.12	6.07	7.69	7.77	7.75	7.71	7.73
NiO	≤0.00	≤0.00	0.33	0.34	0.11	0.10	0.36	0.33	0.36	0.00	0.00	0.02	0.37	0.36	0.36	0.36	0.36
MnO	0.01	≤0.00	0.11	0.14	0.11	0.11	0.11	0.11	0.11	0.04	0.02	0.13	0.11	0.10	0.11	0.11	0.11
MgO	0.01	0.01	50.80	49.84	36.31	36.48	51.54	51.01	51.11	0.01	0.00	14.27	51.33	50.99	50.86	52.17	50.30
CaO	≤0.00	0.00	0.02	0.03	0.42	0.53	0.05	0.05	0.04	0.00	0.01	22.82	0.02	0.04	0.03	0.02	0.04
Na_2O	0.01	0.01	0.02	0.02	0.05	0.04	0.01	0.01	0.01	0.01	0.00	1.10	0.01	0.01	0.01	0.02	0.02
K_2O	≤0.00	0.00	0.00	0.00	≤0.00	≤0.00	0.00	≤0.00	≤0.00	0.04	0.01	≤0.00	≤0.00	≤0.00	≤0.00	≤0.00	≤0.00
Total	102.30	99.84	99.52	99.62	99.01	97.36	101.14	101.84	98.54	100.87	103.10	99.09	100.11	100.58	100.61	102.00	99.48
Si	1.00	1.00	1.00	1.02	1.97	1.93	0.99	1.01	0.97	0.99	0.99	1.95	0.98	1.00	1.00	0.99	1.00
Ti	≤0.00	≤0.00	≤0.00	≤0.00	≤0.00	≤0.00	≤0.00	≤0.00	≤0.00	≤0.00	≤0.00	0.05	≤0.00	≤0.00	≤0.00	≤0.00	≤0.00
Al	≤0.00	≤0.00	≤0.00	≤0.00	0.02	0.02	≤0.00	≤0.00	≤0.00	≤0.00	≤0.00	0.04	≤0.00	≤0.00	≤0.00	≤0.00	≤0.00
Cr	≤0.00	≤0.00	≤0.00	≤0.00	0.01	0.01	≤0.00	≤0.00	≤0.00	≤0.00	≤0.00	≤0.00	≤0.00	≤0.00	≤0.00	≤0.00	≤0.00
Fe2 +	≤0.00	≤0.00	0.15	0.15	0.13	0.13	0.15	0.15	0.16	0.01	0.01	0.19	0.16	0.16	0.16	0.15	0.16
Ni	≤0.00	≤0.00	0.01	0.01	≤0.00	≤0.00	0.01	0.01	0.01	≤0.00	≤0.00	≤0.00	0.01	0.01	0.01	0.01	0.01
Mn	≤0.00	≤0.00	≤0.00	≤0.00	≤0.00	≤0.00	≤0.00	≤0.00	≤0.00	≤0.00	≤0.00	≤0.00	≤0.00	≤0.00	≤0.00	≤0.00	≤0.00
Mg	≤0.00	≤0.00	1.85	1.81	1.87	1.92	1.85	1.81	1.89	≤0.00	≤0.00	0.80	1.86	1.84	1.83	1.85	1.83
Ca	≤0.00	≤0.00	≤0.00	≤0.00	0.02	0.02	≤0.00	≤0.00	≤0.00	≤0.00	≤0.00	0.92	≤0.00	≤0.00	≤0.00	≤0.00	≤0.00
Na	≤0.00	≤0.00	≤0.00	≤0.00	≤0.00	≤0.00	≤0.00	≤0.00	≤0.00	≤0.00	≤0.00	0.08	≤0.00	≤0.00	≤0.00	≤0.00	≤0.00
K	≤0.00	≤0.00	≤0.00	≤0.00	≤0.00	≤0.00	≤0.00	≤0.00	≤0.00	≤0.00	≤0.00	≤0.00	≤0.00	≤0.00	≤0.00	≤0.00	≤0.00
Total	1.00	1.00	3.00	2.98	4.02	4.05	3.01	2.98	3.03	1.01	1.00	4.02	3.02	3.00	3.00	3.01	3.00
Oxygens	2.00	2.00	4.00	4.00	6.00	6.00	4.00	4.00	4.00	2.00	2.00	6.00	4.00	4.00	4.00	4.00	4.00
Mg#			92.60	92.33	93.56	93.60	92.29	92.34	92.30			80.72	92.25	92.13	92.12	92.34	92.07

Diamond	13547b											13803b	13803c	13804b		13805a	
Inclusion	-5	-6a	-7	-9	-10	-11	-13	-14	-15	-16	-112a	-1	-3	-1	2	-1	-2
Mineral	Olv	Olv	Olv	Olv	Olv	Olv	Olv	Olv	Olv	Olv	Olv	Chr	SiO_2	Olv	Olv	Olv	Olv
Paragen.	p	p	p	p	p	p	p	p	p	p	p	p	?	p	p	p	p
Assem.	olv	olv	olv	olv	olv	olv	olv	olv	olv	olv	olv	chr	SiO_2	olv	olv	olv	olv
SiO_2	40.64	40.44	40.95	40.84	40.91	40.80	40.90	40.89	39.28	41.27	39.77	0.11	100.56	40.57	40.92	41.57	40.42
TiO_2	≤0.00	0.00	0.00	0.01	0.00	0.01	0.00	0.01	≤0.00	0.01	≤0.00	0.04	≤0.00	0.01	≤0.00	≤0.00	0.01
Al_2O_3	0.01	0.00	0.02	0.01	0.02	0.01	0.02	0.02	0.01	0.01	0.00	5.79	0.07	0.03	0.03	0.02	0.02
Cr_2O_3	0.06	0.04	0.07	0.04	0.06	0.07	0.08	0.07	0.06	0.07	0.03	65.81	0.01	0.08	0.06	0.03	0.01
FeO	7.63	7.68	7.77	7.66	7.62	7.64	7.74	7.50	7.75	7.66	7.65	15.29	1.20	7.32	7.30	6.68	6.56
NiO	0.35	0.36	0.36	0.37	0.35	0.34	0.37	0.33	0.36	0.36	0.36	0.10	≤0.00	0.35	0.36	0.33	0.32
MnO	0.11	0.11	0.10	0.11	0.11	0.11	0.12	0.11	0.11	0.11	0.12	0.40	0.03	0.11	0.10	0.11	0.11
MgO	52.36	51.11	50.95	50.53	51.21	50.70	51.23	51.60	51.79	51.43	51.73	13.87	≤0.00	51.43	50.60	50.64	50.78
CaO	0.04	0.02	0.04	0.02	0.04	0.04	0.04	0.03	0.04	0.04	0.03	≤0.00	≤0.00	0.02	0.03	0.01	0.01
Na_2O	0.01	0.01	0.02	0.01	0.01	0.02	0.00	0.01	0.01	0.02	0.00	0.01	0.01	0.02	0.02	0.02	0.02
K_2O	0.00	≤0.00	≤0.00	≤0.00	≤0.00	≤0.00	≤0.00	0.01	≤0.00	≤0.00	≤0.00	≤0.00	≤0.00	≤0.00	≤0.00	0.00	0.00
Total	101.23	99.79	100.29	99.60	100.35	99.75	100.49	100.57	99.42	101.00	99.70	101.67	101.90	99.94	99.42	99.44	98.25
Si	0.98	0.99	0.99	1.00	0.99	0.99	0.99	0.99	0.97	0.99	0.97	0.00	0.99	0.99	1.00	1.01	1.00
Ti	≤0.00	≤0.00	≤0.00	≤0.00	≤0.00	≤0.00	≤0.00	≤0.00	≤0.00	≤0.00	≤0.00	≤0.00	≤0.00	≤0.00	≤0.00	≤0.00	≤0.00
Al	≤0.00	≤0.00	≤0.00	≤0.00	≤0.00	≤0.00	≤0.00	≤0.00	≤0.00	≤0.00	≤0.00	0.22	≤0.00	≤0.00	≤0.00	≤0.00	≤0.00
Cr	≤0.00	≤0.00	≤0.00	≤0.00	≤0.00	≤0.00	≤0.00	≤0.00	≤0.00	≤0.00	≤0.00	1.70	≤0.00	≤0.00	≤0.00	≤0.00	≤0.00
Fe2 +	0.15	0.16	0.16	0.16	0.15	0.16	0.16	0.15	0.16	0.15	0.16	0.42	0.01	0.15	0.15	0.14	0.14
Ni	0.01	0.01	0.01	0.01	0.01	0.01	0.01	0.01	0.01	0.01	0.01	≤0.00	≤0.00	0.01	0.01	0.01	0.01
Mn	≤0.00	≤0.00	≤0.00	≤0.00	≤0.00	≤0.00	≤0.00	≤0.00	≤0.00	≤0.00	≤0.00	0.01	≤0.00	≤0.00	≤0.00	≤0.00	≤0.00
Mg	1.88	1.86	1.84	1.84	1.85	1.84	1.85	1.86	1.90	1.85	1.89	0.67	≤0.00	1.86	1.84	1.83	1.86
Ca	≤0.00	≤0.00	≤0.00	≤0.00	≤0.00	≤0.00	≤0.00	≤0.00	≤0.00	≤0.00	≤0.00	≤0.00	≤0.00	≤0.00	≤0.00	≤0.00	≤0.00
Na	≤0.00	≤0.00	≤0.00	≤0.00	≤0.00	≤0.00	≤0.00	≤0.00	≤0.00	≤0.00	≤0.00	≤0.00	≤0.00	≤0.00	≤0.00	≤0.00	≤0.00
K	≤0.00	≤0.00	≤0.00	≤0.00	≤0.00	≤0.00	≤0.00	≤0.00	≤0.00	≤0.00	≤0.00	≤0.00	≤0.00	≤0.00	≤0.00	≤0.00	≤0.00
Total	3.02	3.01	3.01	3.00	3.01	3.01	3.01	3.01	3.03	3.01	3.03	3.03	1.01	3.01	3.00	2.99	3.00
Oxygens	4.00	4.00	4.00	4.00	4.00	4.00	4.00	4.00	4.00	4.00	4.00	4.00	2.00	4.00	4.00	4.00	4.00
Mg#	92.44	92.23	92.12	92.16	92.30	92.21	92.19	92.46	92.26	92.29	92.34	61.79		92.61	92.52	93.11	93.24

Table 1 (*continued*)

Diamond	13805a									
Inclusion	-3	-4	-5	-6	-7	-9b	-10	-12	-13	-15
Mineral	Olv	Olv	Olv	Olv	Olv	Olv	Olv	Olv	Olv	Olv
Paragen.	p	p	p	p	p	p	p	p	p	p
Assem.	olv	olv	olv	olv	olv	olv	olv	olv	olv	olv
SiO_2	41.07	40.82	40.67	41.00	41.06	42.40	40.70	41.43	40.92	40.18
TiO_2	≤0.00	≤0.00	≤0.00	≤0.00	0.01	≤0.00	0.00	0.00	≤0.00	0.01
Al_2O_3	0.01	0.04	0.03	0.01	0.01	0.03	0.01	0.02	≤0.00	≤0.00
Cr_2O_3	0.02	0.04	0.03	0.02	0.03	0.03	0.04	0.03	0.03	0.04
FeO	6.43	6.68	6.37	6.54	6.56	6.64	6.77	6.64	6.68	6.71
NiO	0.33	0.33	0.33	0.32	0.33	0.31	0.31	0.31	0.32	0.34
MnO	0.09	0.09	0.10	0.10	0.10	0.09	0.10	0.10	0.09	0.09
MgO	51.49	51.19	51.94	51.36	51.14	49.80	51.45	53.43	50.64	51.14
CaO	0.01	0.01	≤0.00	0.01	0.01	0.01	0.01	0.02	0.01	0.02
Na_2O	0.02	0.02	0.02	0.01	0.01	0.02	0.02	0.01	0.02	0.01
K_2O	≤0.00	≤0.00	0.01	≤0.00	≤0.00	≤0.00	≤0.00	≤0.00	≤0.00	≤0.00
Total	99.48	99.24	99.50	99.40	99.26	99.32	99.41	101.99	98.71	98.55
Si	1.00	1.00	0.99	1.00	1.00	1.03	0.99	0.98	1.00	0.99
Ti	≤0.00	≤0.00	≤0.00	≤0.00	≤0.00	≤0.00	≤0.00	≤0.00	≤0.00	≤0.00
Al	≤0.00	≤0.00	≤0.00	≤0.00	≤0.00	≤0.00	≤0.00	≤0.00	≤0.00	≤0.00
Cr	≤0.00	≤0.00	≤0.00	≤0.00	≤0.00	≤0.00	≤0.00	≤0.00	≤0.00	≤0.00
Fe2+	0.13	0.14	0.13	0.13	0.13	0.13	0.14	0.13	0.14	0.14
Ni	0.01	0.01	0.01	0.01	0.01	0.01	0.01	0.01	0.01	0.01
Mn	≤0.00	≤0.00	≤0.00	≤0.00	≤0.00	≤0.00	≤0.00	≤0.00	≤0.00	≤0.00
Mg	1.86	1.86	1.88	1.86	1.86	1.80	1.87	1.89	1.85	1.87
Ca	≤0.00	≤0.00	≤0.00	≤0.00	≤0.00	≤0.00	≤0.00	≤0.00	≤0.00	≤0.00
Na	≤0.00	≤0.00	≤0.00	≤0.00	≤0.00	≤0.00	≤0.00	≤0.00	≤0.00	≤0.00
K	≤0.00	≤0.00	≤0.00	≤0.00	≤0.00	≤0.00	≤0.00	≤0.00	≤0.00	≤0.00
Total	3.00	3.00	3.01	3.00	3.00	2.97	3.01	3.02	3.00	3.01
Oxygens	4.00	4.00	4.00	4.00	4.00	4.00	4.00	4.00	4.00	4.00
Mg#	93.45	93.18	93.56	93.33	93.29	93.04	93.13	93.49	93.11	93.14

Diamond	12006b	
Intrusion	-7	-6
Mineral	Pyr.	Pyr.
Paragen.	e	e
Assem.	FeS	FeS
Cr	0.01	≤0.00
Mn	≤0.00	≤0.00
Ni	0.16	0.06
Zn	≤0.00	≤0.00
Mo	0.59	0.59
Cu	0.01	0.02
Co	0.06	0.05
Ti	≤0.00	≤0.00
As	0.03	0.03
Fe	61.92	61.85
S	37.24	37.80
Total	100.03	100.37

xenocrysts from the Renard kimberlites ($Mg\#_{Ca\_corr}$ 84.9 to 90.5 with a mean of 86.9; Hunt, 2011). The values are also typical for harzburgitic inclusions in diamond worldwide (Stachel and Harris, 2008).

5.2.1.4. Clinopyroxene. One clinopyroxene inclusion (from diamond 13532a) was recovered together with an orthopyroxene indicating a lherzolitic or websteritic paragenesis. High Mg# of both the orthopyroxene (93.0) and clinopyroxene (94.9) suggest a peridotitic paragenesis. The Cr_2O_3 content of the clinopyroxene is very low (0.19 wt.%) being more typical of an eclogitic paragenesis (Table 1). However, a very high Cr# (100*Cr/[Cr + Al]) of 79.2 clearly testifies to a lherzolitic origin, with low Cr and Al contents likely being a reflection of unusually low alkalis, allowing for only very low kosmochlor and jadeite components.

5.2.1.5. Spinel. Twenty-five spinel group inclusions were recovered from seven diamonds. They all classify as Mg-chromites with Mg# between 61.8 and 70.1 (mean 66.8) and Cr# between 84.3 and 88.4 (mean 85.8) (Table 1). This is normal for Mg-chromite inclusions in diamonds from worldwide sources (Stachel and Harris, 2008).

5.2.1.6. Sulphides. Two sulphides were recovered from one diamond (12006b). The inclusions are almost pure iron sulphide (Fe: 61.8 and 62.0 wt.%; S: 37.8 and 37.0 wt.%, respectively) (Table 1). A Ni and Cu rich rim is identified in element maps (Fig. 3) but is too thin and, being at the grain edge, also too strongly affected by relief to allow for a fully quantitative analysis. It is assumed that the inclusions initially precipitated as Mss (monosulphide solid solutions) but subsequently exsolved into pyrrhotite (FeS) within the core, with Ni and Cu concentrating in the rim.

Bulanova et al. (1996), building on work by Yefimova et al. (1983), suggested that the Ni content of sulphides may be used to assign paragenesis, with peridotitic sulphide inclusions having high (22–36 wt.%), and eclogitic inclusions low (<12 wt.%), Ni contents. With a bulk Ni content of ~0.1 and 0.2 wt.%, the two sulphides recovered here are clearly eclogitic.

There are large differences in thermal expansion between diamond and Mss (e.g. Birch et al., 1942; Clark, 1966). On cooling, during kimberlite ascent and emplacement, this causes the Mss to increase in volume relative to the host diamond, creating a halo of cracks around the inclusion, as is observed here. Cooling also causes the Mss to undergo exsolution into different phases, including pyrrhotite, pentlandite, chalcopyrite and pyrite (Harris, 1992; Kullerud et al., 1969; Taylor and Liu, 2009; Yefimova et al., 1983). Taylor and Liu (2009) showed that Cu and Ni often concentrate around the edges and in the expansion cracks, similar to what is seen for the sulphides analysed here.

5.2.1.7. SiO_2 phases. Fifteen SiO_2 inclusion phases were recovered from nine Renard diamonds: 12014, 12018, 12036a, 12036b, 13521b, 13521c, 13533, 13539b and 13803c. Coesite inclusions have been observed as minor phases at other localities (e.g. Kopylova et al., 1997; Sobolev et al., 1998; Stachel et al., 1998a), however, such a high abundance at one locality is very unusual. The inclusions were identified prior to breakage of their diamond hosts, and imposed cubo-octahedral morphologies were observed after breakage, indicating syngenetic origins.

Raman spectroscopy was performed on the inclusions to determine the structure of the SiO_2 phases. Ten of the inclusions had the characteristic peaks of coesite (Fig. 4) whilst the remaining five were identified as quartz. Although there were no visible surface fractures, small fractures coated in graphite surrounding four of these quartz inclusions were visible and as such the inclusions likely represent polymorphic transformation from primary coesite during, or subsequent to, exhumation from mantle depth. A detailed view of the fifth quartz inclusion was not possible before breakage due to surface features of the diamond, but based on the above findings is also likely retrograde quartz.

Coesite is associated with olivine in three diamonds and with orthopyroxene in a further one. Whilst all the inclusions were observed prior to breakage of the host diamonds, as SiO_2 phases, olivine and orthopyroxene all appear colourless when included, the spatial relationships between them are unclear.

5.2.2. Epigenetic inclusions

5.2.2.1. Carbonate. Twenty-seven calcite inclusions, with Ca# (100*Ca/[Ca + Mg]) ranging from 97.0 to 100.0, were recovered from seven diamonds (Appendix B1).

Carbonate inclusions have previously been discovered at other localities. Calcite inclusions were reported by Leung (1984) and Meyer and McCallum (1986), magnesite was described by Phillips and Harris (1995), Phillips et al. (2004) and Wang et al. (1996), siderite was found by Stachel et al. (2000) and dolomite by Stachel et al. (1998a), although carbonates were never encountered in such high abundance.

Typically, calcite inclusions in diamond have an epigenetic origin, as in a peridotitic environment, magnesite rather than calcite is expected as the stable carbonate phase at the conditions of diamond formation (Wyllie, 1978; Wyllie and Huang, 1976). Although no fractures were observed in the host diamonds, connecting the inclusion to the surface, such features may have been obscured due to strong relief on diamond surfaces causing poor transparency.

5.2.2.2. Phlogopite. Three phlogopite inclusions were collected from one diamond and a fourth was recovered touching with clinopyroxene, from a second (Appendix B1). Although phlogopite has been found as rare syngenetic inclusions in diamond (e.g. Sobolev et al., 2009 and references therein), unequivocally establishing a primary or secondary origin for phlogopite inclusions is extremely difficult.

The phlogopite compositions are compared to phlogopite analysed from the Renard kimberlites (data from Birkett et al., 2004; Patterson et al., 2009). Birkett et al. (2004) identified a population of kimberlitic phlogopite grains which plotted along a line of decreasing Al and Ti, indentified as a late stage crystallisation trend. Whilst the bulk of Renard kimberlitic phlogopite compositionally fall within the kimberlite field in FeO_T–Al_2O_3 and TiO_2–Al_2O_3 space (Mitchell, 1997; Mitchell et al., 1999), a number also fall along the late stage trend of Birkett et al. (2004). Based on the similarities between the phlogopite inclusions and kimberlitic phlogopite from Renard an epigenetic origin is suggested.

5.2.2.3. Clinopyroxene. Two clinopyroxenes (one touching with phlogopite as discussed above) were recovered from one diamond and are thought to be epigenetic (Appendix B1). Both clinopyroxenes showed large internal chemical heterogeneity and, overall, are compositionally similar to late stage kimberlitic clinopyroxene observed in the Renard kimberlites (Patterson et al. 2009).

5.2.2.4. Amphibole. Three inclusions of amphibole were identified in two diamonds (Appendix B1). The inclusions showed internal heterogeneity, and appeared altered in back scattered electron (BSE) images, indicating an epigenetic origin. The first amphibole has concentrations of 5.1 wt.% CaO, 6.1 wt.% Na_2O, 1.3 wt.% TiO_2, 2.3 wt.% K_2O, 22.44 wt.% MgO and 2.8 wt.% FeO. Using the programme WinAmphcal (Yavuz, 2007) the inclusion is identified as potassium–richterite. The two remaining amphiboles have concentrations of 2.0–2.4 wt.% CaO, 6.5–6.3 wt.% Na_2O, 1.3–1.2 wt.% TiO_2, 1.7–1.8 wt.% K_2O, 20.2–19.9 wt.% MgO and 5.7–5.5 wt.% FeO respectively. The ferric/ferrous iron proportions were not measured and for this composition the final classification is dependent on the ferric iron content of the amphiboles. However, the inclusions likely compositionally lie in the richterite group (WinAmphcal: Yavuz, 2007).

5.2.2.5. Altered sulphides. Seven altered sulphide inclusions were observed in four diamonds. Accurate determinations of composition were not possible due to the alteration so identification was made based on element maps. The remnant sulphides are predominantly composed of Fe, Ni and S (Fig. 5).

Melt/fluid infiltration along grain boundaries and fractures is evident, with the remaining sulphide exhibiting exsolution textures (Fig. 5). The majority of the cavity occupied by the original sulphide inclusion is now filled with calcite and minor apatite, chromite, magnesite, dolomite, spinel and titanite (Fig. 5). This indicates open system behaviour.

5.2.2.6. Djerfisherite-bearing inclusion. A polymineralic inclusion containing djerfisherite (a K-rich sulphide), calcite, dolomite and apatite was identified in one diamond (Fig. 5). The majority of the inclusion is calcite, with apatite, a single crystal of djerfisherite and a single crystal of dolomite. The apatite and dolomite exhibit euhedral crystal shapes, whilst the djerfisherite is subhedral with slightly irregular grain edges.

Due to the crystal habit the djerfisherite is presumed to be secondary; djerfisherite has, however, also been identified as inclusions in the outer growth zones of diamond (Bulanova et al., 1980). Therefore, the possibility that djerfisherite formed in the mantle has subsequently been altered, as observed for other sulphide inclusions in this study, cannot be completely dismissed.

The djerfisherite grain contains 41.9 wt.% Fe, 11.1 wt.% Ni, 30.0 wt.% S, 9.8 wt.%K and 1.1 wt.% Cl which is in agreement with other mantle derived examples of Ni rich and Cu poor djerfisherite from peridotite xenoliths (e.g. Clarke et al., 1977, 1994; Henderson et al., 1999; Sharygin et al., 2007; Takechi et al., 2000) and inclusions in diamond (Bulanova et al., 1980. This contrasts with occurrences of djerfisherite in sulphide deposits and alkaline rocks which are rich in Cu (Dawson et al., 1992, 1995; Henderson et al., 1999; Mitchell, 1997).

5.3. Nitrogen concentrations and aggregation states

Nitrogen has an ionic radius that is similar to carbon, and consequently is the main substitutional impurity in diamond. The concentrations of nitrogen within diamond vary broadly, from below detection to 5500 at. ppm (Sellschop et al., 1979), but rarely exceed 1400 at. ppm (Stachel et al., 2009). Diamonds with eclogitic inclusions typically have higher nitrogen contents (median: 378 at. ppm) compared to peridotitic samples (median: 72 at. ppm) (c.f. Deines et al., 1989; Stachel, 2007).

Diamonds without measurable nitrogen are classified as Type II (Fig. 6a), whilst those with detectable nitrogen contents are classified as Type I. Type I diamonds may be further subdivided based on the aggregation state of the nitrogen (Evans et al., 1981). Initially, nitrogen substitutes into the diamond lattice as single atoms, with the corresponding diamonds being classified as Type Ib. These diamonds are rare in nature due to the high ambient temperatures in the Earth's mantle which cause the singly substituted nitrogen to rapidly aggregate into pairs of nitrogen (A-centre) (e.g. Taylor et al., 1996). Diamonds which contain >90% of their nitrogen in the A-centre are classified as Type IaA (Fig. 6b). During continued mantle residence the nitrogen pairs may aggregate into rings of four atoms surrounding a vacancy (B-centre) (Davies, 1976; Evans et al., 1981). Diamonds which contain >90% of their nitrogen in B-centres are classified as Type IaB. Type IaAB diamonds contain nitrogen in both aggregation states (10–90% of nitrogen in B-centres) (Fig. 6c). Many of these diamonds have an absorbance peak at ~1370 cm^{-1} associated with platelets (Evans et al., 1981; Woods, 1986) (Fig. 6c).

Renard diamonds have nitrogen contents ranging from below the detection limit to 1619 at. ppm with an average of 146 at. ppm (Table 2, Fig. 7), intermediate between the worldwide average for peridotitic and eclogitic diamonds. The diamonds show a range in aggregation from 0 to 70% B, up to Type IaAB (intermediate aggregation), with no diamonds showing fully aggregated nitrogen (Type IaB). At least two analyses per stone were carried out, and variations within single diamond crystals average ~60 at. ppm but may be as high as ~900 at. ppm. Possible variations with growth from core to rim could not be assessed as nitrogen was measured on cleavage fragments after breakage.

Of the 56 diamonds analysed five classified as Type II with both analyses of the stones containing no detectable nitrogen (Table 2). A further two diamonds contained no nitrogen in one fragment and low but measurable nitrogen (9 and 39 at. ppm) in the second. Type II diamonds are only observed in pipes 2 and 4, and all five samples weigh less than 7.8 mg (<1.2 mm wide) (Appendix A1). The percentage of Type II diamonds is less than that observed worldwide, where Type II diamonds comprise 20% of all samples bearing lithospheric mineral inclusion (Stachel, 2007).

The remaining 51 diamonds contain measurable nitrogen in all fragments (classifying as Type Ia) at varying stages of aggregation (Table 2). Four stones are classified as Type IaA, with nitrogen concentrations between 3 and 1324 at. ppm. The majority of the diamonds (25) are Type IaAB, a further 20 have mixed aggregation states within the same stone. Diamond fragments with Type IaAB aggregation have nitrogen concentrations ranging from 8 to 1619 at. ppm.. Type IaA and IaAB stones are found in all pipes sampled for this study.

The time needed for the transition from the A-centre to the B-centre depends on the absolute nitrogen concentration and time-averaged mantle residence temperatures. Assuming geologically reasonable residence times, the aggregation state of nitrogen in diamonds may thus be used as a geothermometer (Evans and Harris, 1989; Taylor et al., 1990).

The exact residence time for the diamonds is not known. Based on the Neoproterozoic eruption ages of the kimberlites (Birkett et al., 2004; Fitzgerald et al., 2008) and late Archean stabilisation of the SCLM beneath Renard (Hunt, 2011) a mantle residence time of 2 Ga has been assumed. It has been shown that mantle residence temperatures are fairly insensitive to the approximated residence time (Evans and Harris, 1989; Leahy and Taylor, 1997). This is demonstrated in Appendix A1, where a difference of 2 Ga in age (3 Ga compared to 1 Ga) gives a maximum temperature difference of ~30 °C. In the case of pure Type IaA diamonds (0% B) a maximum mantle residence temperature is calculated assuming that an amount of B-defect is present that corresponds to half the detection limit (~0.05%), (see Leahy and Taylor, 1997).

Nitrogen based time averaged mantle residence temperatures (Leahy and Taylor, 1997) give a range from ~1040 to 1230 °C, with

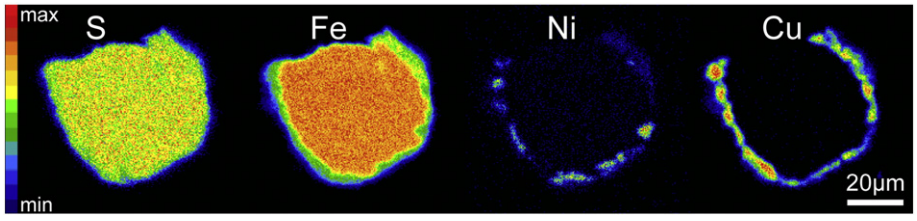

Fig. 3. Microprobe element maps of a zoned sulphide inclusion from diamond 12006b.

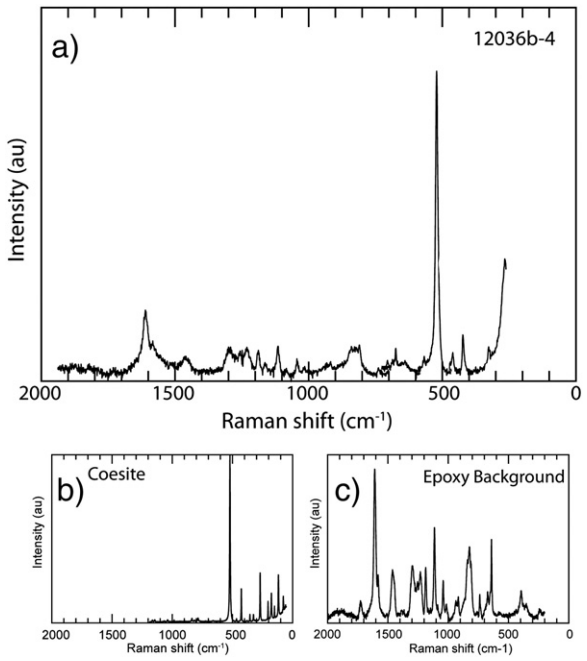

Fig. 4. a) Representative Raman spectrum of a diamond inclusion (12036b-4). b) Typical Coesite spectrum (Handbook of Minerals Raman Spectra; http://www.ens-lyon.fr/LST/Raman/). c) Spectrum of the epoxy in which the inclusion is mounted.

the majority of determined temperatures being between 1100 and 1200 °C (Table 2, Fig. 7). Type IaA diamonds give a cooler temperature range (~1040–1180 °C), compared to the type IaAB diamonds which approximately span the entire temperature range (1065–1230 °C). The diamonds from all pipes, with the exception of pipe 4, have a bimodal distribution in nitrogen averaged mantle residence temperatures: A mode at ~1075–1100 °C (primarily composed of Type IaA stones); and a second mode at ~1150–1200 °C (predominantly composed of Type IaAB stones). Pipe 4 likely sampled different diamond bearing horizons in the SCLM, with only one large mode at 1150–1175 °C. Type IaA diamonds are relatively less abundant in this pipe, and have higher average temperatures than those observed in other pipes, due to very low nitrogen contents. However, as 0.5% aggregation to B centres is assumed for these pure Type IaA diamonds, these are maximum temperature estimates.

5.4. Carbon isotopic composition

Worldwide data show diamonds to have a broad range in stable carbon isotopic composition ($\delta^{13}C$) from −41‰ (De Stefano et al., 2009) to +5‰ (Cartigny, 2005). Peridotitic diamonds are mainly restricted to $\delta^{13}C$ values between −10 and −2‰ whereas eclogitic diamonds have isotopic compositions from −41 (De Stefano et al., 2009) to +2.9‰ (Davies et al., 2003).

The Renard diamonds have a small range in $\delta^{13}C$ of −5.4‰ to −1.2‰. All but four of the diamonds, however, fall within an even narrower range between −4.6‰ and −2.6‰ (Table 4.3, Fig. 8). The distribution of $\delta^{13}C$ has a well-defined mode at −3.25‰ (class −3.5 to −3.0‰). An identical mode in carbon isotopic composition is observed for octahedral diamonds from the Crystal showing at Wawa (Stachel et al., 2006) – a conglomerate hosted diamond deposit on the Superior Craton, ~1000 km SW of Renard (Fig. 8).

No correlation is observed between the physical characteristics (colour, surface features, morphology) and $\delta^{13}C$. No significant differences in carbon isotopic composition are observed among diamonds from the five studied pipes nor among different inclusion assemblages. The latter observation includes the single eclogitic diamond containing two Ni poor sulphide inclusions, with a $\delta^{13}C$ of −3.6‰.

5.5. Thermometry

Three diamonds contained mineral associations suitable for geothermometry. The coexistence of garnet with two olivines in two diamonds (12013 and 13523) allowed for the calculation of equilibrium temperatures based on the Fe–Mg exchange (O'Neill and Wood, 1979). As the inclusions were not in contact, they reflect temperature conditions of diamond formation: 1110–1140 °C and 1170–1180 °C for samples 12013 and 13523, respectively. A third diamond (13532a) contained a single clinopyroxene and a single orthopyroxene. The Ca-in-orthopyroxene thermometer (Brey and Köhler, 1990) gave an equilibrium temperature of 1120 °C. Clinopyroxene based thermobarometers could be utilised due to the unusual composition of the lherzolitic clinopyroxene inclusion, which falls outside calibrated compositional ranges.

6. Discussion

6.1. Diamondiferous SCLM

6.1.1. Diamond source region

Based on our inclusion data, the diamondiferous lithospheric mantle beneath Renard appears to be strongly dominated by peridotite, with only one of 33 inclusion bearing diamonds having an eclogitic origin. This agrees with the xenolith/xenocryst record (Hunt, 2011) which is predominantly peridotitic, with only a minor (3% of the studied samples) eclogitic portion. Of the 32 diamonds with peridotitic inclusions, three are of harzburgitic (two diamonds contain harzburgitic garnets, and a further contains a low Ca orthopyroxene) and two of lherzolitic paragenesis (one with two olivine inclusions with CaO > 0.05 wt.%, the

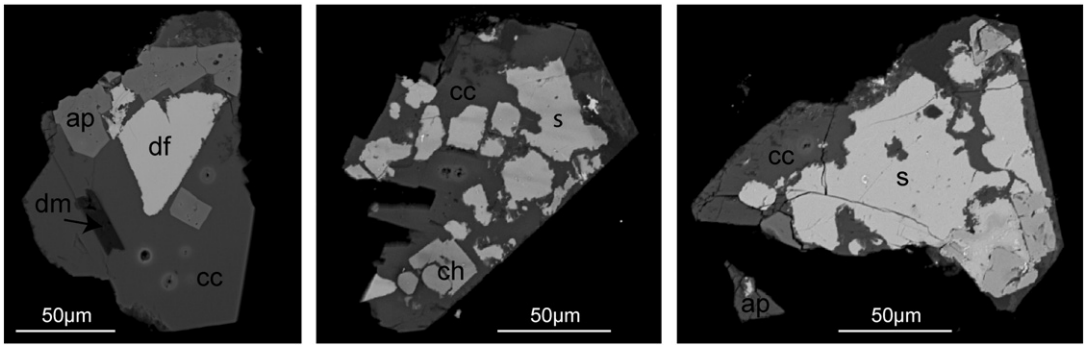

Fig. 5. Back-scattered electron (BSE) images of polymineralic inclusions. df = djerfisherite, s = sulphide (typically pyrrhotite), cc = calcite, dm = dolomite, ap = apatite, chr = chromite.

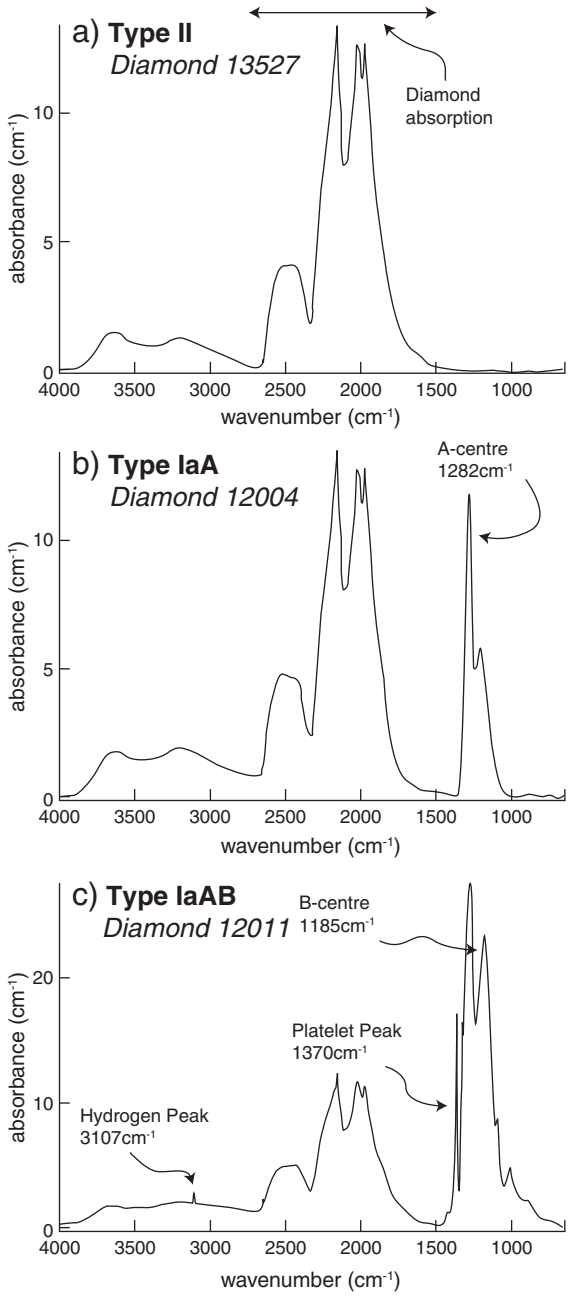

Fig. 6. Absorption coefficient (cm^{-1}) vs. wavenumber for representative FTIR spectra. a) Type II (nitrogen free) diamond spectrum. b) Type IaA diamond spectrum showing the characteristic absorbance at 1282 cm^{-1} (A-centre). c) Type IaAB diamond spectrum showing the additional characteristic absorbance at 1185 cm^{-1} (B-centre). An additional absorbance peak at 1370 cm^{-1} is caused by the presence of platelets.

other containing clinopyroxene and orthopyroxene). For the remaining 88% of peridotitic samples a specific paragenesis cannot be determined.

Major and trace element variations in mantle xenoliths and inclusions in diamond support the view that peridotitic SCLM originated as residues of variable degrees of polybaric melt extraction, ending at relatively low pressures (≤30 kbar) (Kelemen, et al., 1998; Stachel et al., 1998b; Walter, 1999). One of the key pieces of evidence for this is the high Cr# of cratonic peridotites (reflected by Cr rich garnets and Mg-chromites), (e.g., Bulatov et al., 1991; Canil and Wei, 1992; Stachel et al., 1998b). This is consistent with two G10 garnets (Cr# of 26.0 and 29.7) and 25 chromite inclusions (average Cr# of 85.7) studied here, which all imply a source with high Cr#.

The Renard inclusions are extremely magnesian, with an average Mg# of 92.7 for olivine (Fig. 3) and 93.9 for orthopyroxene. A similar average olivine Mg# of ~92.8 has been observed from a number of other independent sources, including: A compilation of cratonic spinel and garnet peridotites (Pearson et al., 2003); indirectly, through estimates of olivine Mg# from kimberlite concentrate garnet chemistry (Gaul et al., 2000); olivine inclusions from peridotitic diamonds from Siberian kimberlites (Sobolev et al., 2004); and a compilation of worldwide olivine diamond inclusions (average Mg# of 92.9) (Stachel and Harris, 2008). High-Mg# peridotite xenoliths have been reported from cratonic areas around the globe, e.g. Siberian, Kaapvaal and Slave cratons (Bernstein et al., 1998, 2006; Bizzarro and Stevenson, 2003; Boyd et al., 1997; Kopylova and Russell, 2000; Lee and Rudnick, 1999; Rudnick et al., 1994). The similarities between the Renard inclusion suite and inclusion suites from other cratonic regions worldwide suggest that they were sourced from similar cratonic mantle.

The observed narrow range of olivine Mg# corresponds to the experimentally determined range (Mg# from 92.8 to 93.0) associated with high degrees (40%–42%) of melt extraction leading to exhaustion of orthopyroxene during mantle melting (Bernstein et al., 2007 and references within). Bernstein et al. (2007) proposed that most, or all, highly depleted cratonic mantle peridotites originated as dunite residues after ≥40% melt extraction, and have since undergone variable amounts of refertilisation. An origin of Renard diamonds from highly melt depleted peridotitic sources is consistent with similar observations worldwide, which are reflected in the strong association between diamonds and G10 (harzburgitic–dunitic) garnets established by Gurney (1984).

In the related study of Hunt (2011), the majority (79%) of microxenoliths from Renard were sampled from a depth range of ~130–160 km, with the deepest samples coming from ~190 km. Projecting the results of inclusion thermometry (1110–1180 °C) on the Neoproterozoic model geotherm of 38 mW/m^2 derived from these microxenoliths, indicates the Renard diamonds originate from a depth of ~175–200 km, i.e. from near the base of the lithosphere. Projecting the nitrogen thermometry data (1040–1230 °C) onto the same geotherm gives a similar depth range of 160–210 km (average 190 km) This implies that the majority of diamonds, for which either inclusion or nitrogen based temperatures are available, appear to derive from greater depths than the bulk of the xenolith record. This may indicate selective sampling of diamonds/xenoliths at different depths. Alternatively, diamond formation a Renard may have been associated with transient heating, as previously observed for diamond suites elsewhere (Phillips et al., 2004; Stachel et al., 2003), rendering projection of inclusion temperatures on kimberlite eruption age paleogeotherms spurious.

6.2. Diamond formation and residence

6.2.1. Diamond source carbon

The carbon isotopic data (−5.4‰ to −1.2‰: Fig. 8) are consistent with the predominantly peridotitic suite defined via mineral inclusions. The mode of −3.25‰ agrees with previous work from the Superior Province (Wawa: Stachel et al., 2006) (Fig. 8). This mode is not observed in other cratonic regions (database of Stachel et al., 2009), and may suggest distinct carbon isotopic sources for diamonds from the Superior craton. The small range in $\delta^{13}C$ for Renard diamonds suggests that the extent of isotopic fractionation is limited, implying an excess of diamond forming melts/fluids.

It is generally accepted that peridotitic diamonds form during redox reactions between either a reduced (e.g. Taylor, 1988) or an oxidized (e.g. Eggler and Baker, 1982; Luth, 1993) fluid/melt and the host peridotite. Stachel et al. (2009) showed that a $d^{13}C$ dataset for inclusion bearing peridotitic diamonds from worldwide source is consistent with Raleigh fractionation during diamond precipitation involving both oxidized and reduced fluids/melts. Using the fractionation factors of

Table 2
The carbon isotopic composition, inclusion thermometry and nitrogen content and aggregation state of the diamonds. Nitrogen mantle residence temperatures have been determined after Leahy and Taylor (1997) for 3Ga (T [N,3Ga]), 2Ga (T [N,2Ga]) and 1Ga (T [N,1Ga]). For poorly aggregated Type IaA diamonds, a maximum mantle residence temperature is calculated assuming 0.05% B-defect (following Leahy and Taylor, 1997). Type IaA - nitrogen content present in the A-centre; Type IaB - nitrogen content present in the B-centre.

Pipe no.	Diamond	Type IaA	Type IaB	N Content (ppm)	%B	Type	T [N, 3Ga]	T [N, 2Ga]	T [N, 1Ga]	Inclusion temp	Carbon $d^{13}C$
1	12026	46.1	0.0	46.1	0.0	IaA	1062	1071	1086	–	–
1	12026	34.4	12.2	46.6	26.2	IaAB	1162	1172	1190	–	−2.71
1	12027	6.2	0.0	6.2	0.0	IaA	1107	1117	1133	–	–
1	12027	5.9	2.0	7.9	25.3	IaAB	1207	1218	1237	–	−2.86
1	12029	18.3	3.5	21.8	16.1	IaAB	1165	1176	1194	–	–
1	12029	56.0	36.0	92.0	39.1	IaAB	1160	1170	1188	–	−4.43
1	12031	15.2	12.0	27.2	44.1	IaAB	1197	1208	1226	–	–
1	12031	13.5	0.0	13.5	0.0	IaA	1089	1099	1115	–	−4.03
2	12036a	27.2	1.5	28.7	5.2	IaA	1128	1138	1155	–	–
2	12036a	22.5	8.4	30.9	27.2	IaAB	1174	1184	1203	–	−3.43
2	12036b	27.1	0.0	27.1	0.0	IaA	1073	1083	1098	–	–
2	12036b	30.0	19.6	49.6	39.5	IaAB	1176	1186	1205	–	−4.49
2	12040	19.5	0.0	19.5	0.0	IaA	1081	1090	1106	–	–
2	12040	18.7	0.0	18.7	0.0	IaA	1082	1091	1107	–	−3.84
2	12041	18.6	0.0	18.6	0.0	IaA	1082	1091	1107	–	–
2	12041	30.8	4.1	34.9	11.7	IaAB	1145	1155	1172	–	−3.50
2	12042	163.8	21.9	185.7	11.8	IaAB	1104	1114	1131	–	–
2	12042	121.5	38.2	159.7	23.9	IaAB	1128	1138	1155	–	−3.64
2	13527	0.0	0.0	0.0	0.0	II	–	–	–	–	–
2	13527	0.0	0.0	0.0	0.0	II	–	–	–	–	−3.46
2	13528a	47.7	26.8	74.5	36.0	IaAB	1162	1172	1190	–	–
2	13528a	82.9	38.8	121.7	31.9	IaAB	1145	1155	1173	–	−3.89
2	13528b	0.0	0.0	0.0	0.0	II	–	–	–	–	–
2	13528b	0.0	0.0	0.0	0.0	II	–	–	–	–	−3.38
2	13803a	28.3	14.7	43.0	34.2	IaAB	1174	1184	1203	–	–
2	13803a	34.8	32.1	66.9	48.0	IaAB	1177	1188	1206	–	−4.35
2	13803b	25.2	25.0	50.2	49.8	IaAB	1186	1197	1216	–	–
2	13803b	22.8	0.0	22.8	0.0	IaA	1077	1086	1102	–	−4.01
2	13803c	0.0	0.0	0.0	0.0	II	–	–	–	–	–
2	13803c	39.0	0.0	39.0	0.0	IaA	1065	1074	1090	–	−3.34
2	13804a	0.0	0.0	0.0	0.0	II	–	–	–	–	–
2	13804a	33.3	0.0	33.3	0.0	IaA	1069	1078	1094	–	–
2	13804a	17.1	4.7	21.8	21.6	IaAB	1175	1185	1204	–	−3.31
2	13804b	77.4	116.8	194.2	60.1	IaAB	1162	1173	1191	–	–
2	13804b	7.5	7.2	14.7	49.0	IaAB	1219	1230	1249	–	−3.74
2	13805a	112.6	59.3	171.9	34.5	IaAB	1139	1149	1167	–	–
2	13805a	94.9	51.0	145.9	35.0	IaAB	1144	1154	1171	–	−3.37
2	13805b	273.3	99.8	373.1	26.7	IaAB	1112	1121	1138	–	–
2	13805b	333.8	115.3	449.1	25.7	IaAB	1106	1116	1132	–	−3.85
3	13530a	45.5	28.6	74.1	38.6	IaAB	1165	1175	1193	–	–
3	13530a	45.1	24.9	70.0	35.6	IaAB	1163	1173	1191	–	−3.06
3	13530b	29.5	0.0	29.5	0.0	IaA	1072	1081	1096	–	–
3	13530b	15.0	8.6	23.6	36.4	IaAB	1192	1203	1222	–	−3.53
3	13530c	7.7	0.7	8.4	8.3	IaA	1171	1181	1200	–	–
3	13530c	20.3	5.7	26.0	21.9	IaAB	1171	1181	1200	–	−3.89
3	13531a	580.1	437.9	1018.0	43.0	IaAB	1105	1115	1131	–	–
3	13531a	408.7	204.7	613.4	33.4	IaAB	1107	1117	1134	–	−5.41
3	13531b	30.6	4.7	35.3	13.3	IaAB	1148	1158	1176	–	–
3	13531b	40.2	0.8	41.0	2.0	IaA	1095	1105	1121	–	−4.38
3	13532a	22.9	7.7	30.6	25.2	IaAB	1171	1182	1200	1122	–
3	13532a	35.1	15.2	50.3	30.2	IaAB	1165	1175	1194	–	−3.71
3	13532b	48.9	31.5	80.4	39.2	IaAB	1163	1174	1192	–	–
3	13532b	50.3	29.4	79.7	36.9	IaAB	1161	1171	1189	–	−3.37
3	13533	46.2	20.5	66.7	30.7	IaAB	1158	1169	1187	–	–
3	13533	22.3	17.5	39.8	44.0	IaAB	1186	1197	1216	–	−4.47
4	13520	23.6	15.3	38.9	39.3	IaAB	1182	1193	1211	–	–
4	13520	12.8	1.5	14.3	10.5	IaAB	1164	1174	1192	–	−4.35
4	13521a	0.0	0.0	0.0	0.0	II	–	–	–	–	–
4	13521a	0.0	0.0	0.0	0.0	II	–	–	–	–	-3.10
4	13521b	1417.5	201.8	1619.3	12.5	IaAB	1057	1066	1081	–	–
4	13521b	1274.5	49.3	1323.8	3.7	IaA	1033	1042	1057	–	-4.08
4	13521c	30.2	38.8	69.0	56.2	IaAB	1185	1196	1214	–	–
4	13521c	11.8	4.4	16.2	27.2	IaAB	1191	1201	1220	–	-3.08
4	13523	36.2	13.6	49.8	27.3	IaAB	1162	1172	1190	1177	–
4	13523	37.6	10.2	47.8	21.3	IaAB	1154	1165	1183	1170	-3.65
4	13524	0.0	0.0	0.0	0.0	II	–	–	–	–	–
4	13524	0.0	0.0	0.0	0.0	II	–	–	–	–	-3.39
4	13536	3.1	0.0	3.1	0.0	IaA	1124	1133	1151	–	–
4	13536	7.3	2.7	10.0	27.0	IaAB	1203	1214	1233	–	-2.09
4	13537	8.0	0.9	8.9	10.1	IaAB	1175	1185	1204	–	–
4	13537	0.0	0.0	0.0	0.0	II	–	–	–	–	-3.51
4	13538	7.8	0.0	7.8	0.0	IaA	1102	1111	1128	–	–

Table 2 (*continued*)

Pipe no.	Diamond	Type IaA	Type IaB	N Content (ppm)	%B	Type	T [N, 3Ga]	T [N, 2Ga]	T [N, 1Ga]	Inclusion temp	Carbon $d^{13}C$
4	13538	30.2	0.0	30.2	0.0	IaA	1071	1080	1096	–	-3.53
4	13539a	9.5	0.0	9.5	0.0	IaA	1097	1107	1123	–	–
4	13539a	9.3	1.2	10.5	11.4	IaAB	1174	1185	1203	–	-3.66
4	13539b	81.8	11.6	93.4	12.4	IaAB	1122	1132	1149	–	–
4	13539b	67.6	8.8	76.4	11.5	IaAB	1125	1135	1152	–	-2.86
4	13540	272.1	228.1	500.2	45.6	IaAB	1124	1134	1151	–	–
4	13540	319.4	109.5	428.9	25.5	IaAB	1107	1116	1133	–	-3.49
4	13544	58.0	40.9	98.9	41.4	IaAB	1160	1171	1189	–	–
4	13544	65.0	6.2	71.2	8.7	IaA	1119	1129	1146	–	-5.35
4	13545	44.6	22.5	67.1	33.5	IaAB	1162	1172	1190	–	–
4	13545	46.9	31.9	78.8	40.5	IaAB	1165	1175	1194	–	-3.16
4	13547a	0.0	0.0	0.0	0.0	II	–	–	–	–	–
4	13547a	0.0	0.0	0.0	0.0	II	–	–	–	–	-4.08
4	13547b	116.4	239.0	355.4	67.2	IaAB	1155	1165	1183	–	–
4	13547b	112.1	227.4	339.5	67.0	IaAB	1156	1166	1184	–	-3.94
4	13548	476.8	316.4	793.2	39.9	IaAB	1108	1118	1134	–	–
4	13548	544.2	317.6	861.8	36.9	IaAB	1103	1113	1129	–	-3.28
65	12001	210.8	124.9	335.7	37.2	IaAB	1126	1136	1153	–	–
65	12001	188.1	115.4	303.5	38.0	IaAB	1129	1139	1156	–	-1.19
65	12003	16.9	0.0	16.9	0.0	IaA	1084	1093	1109	–	–
65	12003	17.7	5.9	23.6	25.0	IaAB	1178	1188	1207	–	-3.95
65	12004	220.5	0.0	220.5	0.0	IaA	1028	1037	1051	–	–
65	12004	197.1	0.0	197.1	0.0	IaA	1031	1039	1054	–	-2.82
65	12006a	145.6	5.9	151.5	3.9	IaA	1082	1091	1107	–	–
65	12006a	163.0	6.0	169.0	3.6	IaA	1077	1086	1102	–	-3.09
65	12006b	119.9	22.1	142.0	15.6	IaAB	1118	1128	1145	–	–
65	12006b	483.4	547.4	1030.8	53.1	IaAB	1114	1124	1141	–	–
65	12006b	392.0	328.2	720.2	45.6	IaAB	1116	1125	1142	–	-3.64
65	12011	38.6	49.8	88.4	56.3	IaAB	1179	1189	1208	–	–
65	12011	313.2	216.6	529.8	40.9	IaAB	1118	1128	1145	–	-3.01
65	12012	23.4	3.6	27.0	13.3	IaAB	1155	1165	1183	–	–
65	12012	25.7	0.4	26.1	1.5	IaA	1100	1110	1126	–	-3.28
65	12013	75.5	197.1	272.6	72.3	IaAB	1168	1178	1196	1140	–
65	12013	16.7	13.5	30.2	44.7	IaAB	1195	1205	1224	1110	–
65	12013	33.0	0.0	33.0	0.0	IaA	1069	1078	1094	–	-3.38
65	12014	77.3	44.3	121.6	36.4	IaAB	1150	1160	1178	–	–
65	12014	40.6	4.5	45.1	10.0	IaA	1134	1144	1161	–	-3.48
65	12016a	57.1	12.0	69.1	17.4	IaAB	1139	1149	1166	–	–
65	12016a	62.8	38.3	101.1	37.9	IaAB	1156	1166	1184	–	-4.70
65	12016b	57.8	14.1	71.9	19.6	IaAB	1142	1152	1169	–	–
65	12016b	38.8	0.0	38.8	0.0	IaA	1065	1074	1090	–	-4.53
65	12018	40.5	18.8	59.3	31.7	IaAB	1163	1173	1191	–	–
65	12018	30.6	7.4	38.0	19.5	IaAB	1157	1168	1186	–	-2.69

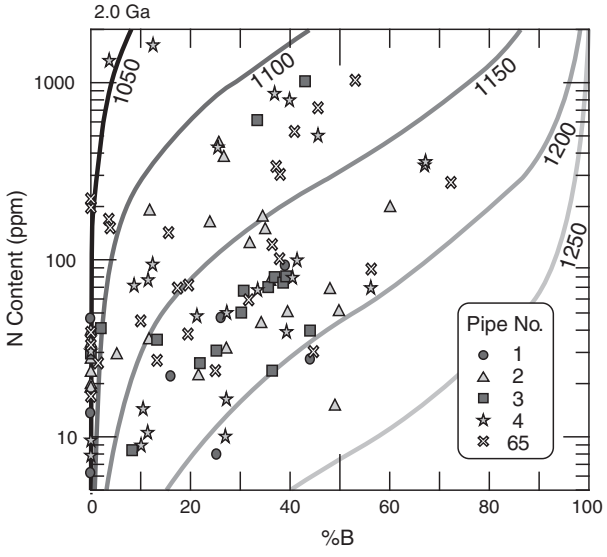

Fig. 7. Time averaged mantle residence temperatures determined from nitrogen content and aggregation state. Nitrogen aggregation (%B) is expressed as the relative proportion of nitrogen in the B centre. Isotherms based on 2 Ga mantle residence times are calculated after Taylor et al. (1990) and Leahy and Taylor (1997). For good spectra, 1 sigma errors for %B at ±5% (absolute), errors of N content typically are smaller than the symbol size (~10% below 500 ppm, 5% above 500 ppm).

Polyakov and Kharlashina (1995) for diamond and a carbonatitic fluid/melt, Richet et al. (1977) for diamond and a methane bearing fluid/melt, and Chacko et al. (1991) for diamond and a CO_2 melt/fluid, possible diamond forming fluids/melts for the Renard diamonds were determined. Similar to the conclusions of Stachel et al. (2009), precipitation of

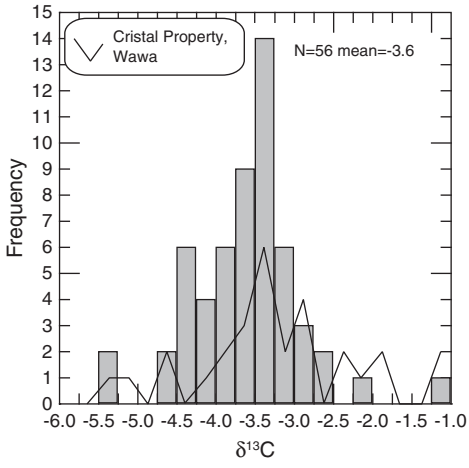

Fig. 8. Carbon isotopic compositions of Renard diamonds. The black line represents data from the Crystal showing at Wawa (Stachel et al., 2006) shown for comparison.

Renard diamonds may have involved CH_4 ($\delta^{13}C$ of crystallising diamond decreases) and/or CO_3^{2-} and CO_2 ($\delta^{13}C$ of crystallising diamond increases) bearing fluids/melts. CO_2 is buffered by carbonation reactions in olivine bearing rocks at high pressure (Wyllie and Huang, 1976) and, therefore, it is not likely to be a significant diamond forming agent. However, as discussed below, the coesite inclusions in Renard diamonds could result from such carbonation reactions involving a free CO_2 fluid.

Precipitation of Renard diamonds, with carbon isotopic values in the range of −5.4‰ to −1.2‰, can be explained by involving two carbon bearing fluids/melts. (1.) A methane bearing melt/fluid with an initial carbon isotopic composition ($\delta^{13}C_0$) of approximately −4.5‰ (i.e., within the mantle range of -5 ± 1‰, e.g. Cartigny, 2005) will precipitate diamonds with initial δ^{13} of −3.6‰, which will become progressively lighter through fractionation. (2.) From oxidising melts/fluids: Diamonds crystallising from a $\delta^{13}C_0$ of −2.2‰ (CO_3^{2-}) and −0.3‰ (CO_2) will lead to precipitation of diamonds with an initial $\delta^{13}C$ of −3.8‰, which will become progressively heavier through fractionation. This range for $\delta^{13}C_0$ for oxidized media is consistent with the carbon isotopic composition of subducted marine carbonates ($\delta^{13}C_0$ of 0 +/− 5‰; Schidlowski et al., 1983). Progressive devolatilisation during subduction will drive their isotopic composition towards lower and hence more mantle-like $\delta^{13}C$ values (Stachel et al., 2009).

6.3. Geothermobarometry

Time averaged mantle residence temperatures based on diamond nitrogen contents and aggregation states agree with worldwide peridotitic diamond data (database of Stachel and Harris, 2008). Both data sets have single modes, occurring in class 1150–1175 °C, and almost identical averages (1145 vs. 1155 °C for Renard and the 835 peridotitic diamonds worldwide, respectively; see Fig. 9). The Renard diamonds, therefore, resided in a mantle environment typical for peridotitic diamonds from other cratonic regions, with kimberlite sampling occurring over the entire depth range of diamond stable lithospheric mantle.

Temperatures calculated from mineral inclusion equilibria agree within error to nitrogen based mantle residence temperatures of their associated host diamonds (Table 2). For non-touching inclusion pairs, geothermometry yields temperature conditions during entrapment, i.e. during diamond formation. The overall good agreement between mineral inclusion and nitrogen based temperature estimates, therefore, appears to suggest that formation and mantle residence of Renard diamonds occurred at similar temperatures and that major thermal perturbations during mantle residence did not occur. That this picture of steady state conditions in the eastern Superior SCLM is likely too simplistic on a detailed level is indicated by a subgroup of diamonds that show intra-grain variations in $T_{Nitrogen}$ outside the uncertainty of the method.

Time averaged temperatures do not distinguish between storage at a constant mantle temperature and residence at a relatively lower temperature with intermittent thermal spikes. Uniform $\delta^{13}C$, co-variations in nitrogen concentration and aggregation state yielding nearly constant $T_{Nitrogen}$, and agreement with inclusion thermometry for the majority of individual diamond samples is consistent with one main stage of diamond growth.

Within a subgroup of 13 (out of the 56) Renard diamonds, co-variations in nitrogen content and aggregation state are, however, either absent or do not follow isotherms. This results in apparent differences in residence temperature, from separate fragments of individual stones, of up to 127 °C (Fig. 10), which is considered outside of error. For "normal" FTIR spectra, analytical uncertainties propagated through temperature estimates result in 1 sigma errors of up to ±20 °C (Fig. 10). Taylor et al. (1996) determined errors to be similar to that of conventional geothermobarometry (~50 °C). However, for some diamond fragments, surface characteristics lead to spectra with strongly curved backgrounds, requiring large baseline corrections, based on multiple, subjectively chosen nodes. For such diamonds, the accuracy in the determination of nitrogen contents and aggregation states is poor but cannot be readily quantified. As such, only diamonds with FTIR spectra that required minimal baseline correction and, therefore, associated with minimal analytical error, were considered for an evaluation of intra-sample homogeneity.

Large differences in $T_{Nitrogen}$ within individual diamonds may relate to multiple growth events occurring, either over an extended time period (billions of years), or during thermal relaxation (cooling) following thermal perturbations. Consequently, within individual diamonds, the part with the highest time averaged mantle residence temperature would derive from the centre of the crystal. Alternatively, non-isothermal co-variations in nitrogen content and aggregation state may result from the averaging effect of FTIR analyses for heterogeneous samples (Harte et al., 1999): as the speed of nitrogen aggregation not only depends on temperature but also on nitrogen content, heterogeneous distribution of nitrogen among growth sectors leads to an overestimation of $T_{Nitrogen}$ in FTIR analyses that are not conducted on plates cut parallel {110} or that laterally overlap multiple sectors. However, the observation that large variations in $T_{Nitrogen}$, in most cases, are not associated with significant changes in nitrogen abundance makes this a less likely alternative.

6.4. SCLM modification

6.4.1. Coesite inclusion paragenesis

Microprobe analyses of the Renard diamond inclusions show a dominantly peridotitic suite, consisting of abundant olivine and chromite, and lesser amounts of clinopyroxene, orthopyroxene and garnet. Only one diamond is of likely eclogitic origin, containing two sulphide inclusions of low Ni content. A coesite inclusion assemblage is also identified (Table 1). Coesite is associated with olivine in three diamonds and with orthopyroxene in another. The "coexistence" of olivine and an SiO_2 phase in single diamonds reflects trapping of inclusions during different stages of diamond growth in a changing chemical environment. This is also documented through disequilibrium among multiple olivine inclusions in single diamonds, which show variations in forsterite content up to 0.5, e.g., in diamonds 12036b (ΔFo 0.37), 13547b (ΔFo 0.45) and 13805a (ΔFo 0.45).

The presence of abundant coesite inclusions at Renard is unusual: Worldwide, coesite forms only ~1% of observed inclusions with the majority being eclogitic (74%) and less commonly websteritic and lherzolitic (13% each; Stachel and Harris, 2008). Localities where coesite inclusions of eclogitic paragenesis are relatively abundant are Argyle, Western Australia (Jaques et al., 1989), and the Guaniamo kimberlites, Venezuela (Sobolev et al., 1998).

The low $\delta^{13}C$ values of the Guaniamo diamonds (as low as −28.7‰, with most diamonds in the range −10‰ to −20‰: Kaminsky et al., 2000; Sobolev et al., 1998) and the high $\delta^{18}O$ of the coesite inclusions (10.2–16.9‰: Schulze et al., 2003) has been used to suggest that a subducted crustal component may have contributed to their genesis. The abundance of coesite inclusions is linked to a silica rich growth environment, implying little or no partial melting of the basaltic/eclogitic material in the oceanic slab during, and following, subduction (Schulze et al., 2003).

An alternative explanation, relevant for coesite inclusions in diamonds of peridotitic paragenesis, involves extreme carbonation of their peridotitic sources to create a free SiO_2 phase. In peridotite all olivine must be carbonated before a free SiO_2 phase is stable. Assuming reaction of a typical lherzolitic assemblage of olivine, orthopyroxene, clinopyroxene and garnet with an excess of CO_2, calcic magnesite and SiO_2 (plus residual garnet) are formed (Wyllie and Huang, 1976; Wyllie et al., 1983). The occurrence of free SiO_2 inclusions relating to

extreme carbonation of peridotitic diamond sources was first identified in a diamond from the Mwadui mine (Stachel et al., 1998a).

Complete carbonation of lherzolite involves the addition of >30 wt.% of CO_2 (Schrauder and Navon, 1993). Such extreme CO_2 influx can only occur within localised regions of the lithosphere, for example as fully carbonated metasomatic veins (Schrauder and Navon, 1993).

The source of the CO_2 is difficult to define, however, it may have originated from subducted carbonaceous sediments, or asthenosphere derived melts, as the solubility of CO_2 within the melts increases considerably with increasing pressure. The melts may thus concentrate carbon and release it locally as they ascend (Ballhaus and Frost, 1994; Schrauder and Navon, 1993).

Progressive source carbonation may also explain the presence of typical peridotitic inclusions (olivine and orthopyroxene) together with coesite within single diamonds: Olivine and orthopyroxene would need to be occluded first, prior to complete source carbonation, whilst the coesite inclusions would represent the final product of all successive carbonation reactions.

Alternatively, if coesite was included first, in an eclogitic environment that was subsequently converted, metasomatically, to an olivine websterite, then the chemistry of the olivine and orthopyroxene inclusions should be different: websteritic orthopyroxene inclusions worldwide have an average Mg# of 83.9 +/− 4.0 (1σ) (Stachel and Harris, 2008) and websteritic olivine inclusions (extremely rare and therefore no compositional ranges available), by inference (von Seckendorff and O'Neill, 1993), should fall in the same range. These Mg# are markedly lower than the observed values of 92.4–92.9 for olivine inclusions and 94.6 for orthopyroxene included with coesite. This clearly precludes formation of these diamonds in compositionally evolving coesite eclogites.

6.4.2. Epigenetic inclusions

The presence of highly altered sulphide inclusions partially replaced by carbonate has not been observed in previous diamond inclusion studies. Whilst carbonatitic and sulphide bearing diamond-forming media both exist in the upper mantle, experimental data indicate that at P–T conditions of diamond stability carbonate–silicate and sulphide melts are characterised by complete immiscibility (e.g. Litvin and Butvina, 2004; Litvin et al., 2005; Shushkanova and Litvin, 2005, 2008).

For Renard diamonds, the immiscibility between sulphide and carbonate/silicate melts, and the lack of Fe in the carbonate (identified primarily as calcite) suggest that a two stage open system process, rather than simple replacement of iron sulphide through carbonate, occurred. The first stage is the partial removal of primary sulphide inclusions, and the second stage is the deposition of carbonate. Jugo et al. (2005) showed that sulphur solubility in basaltic melts is strongly dependent on sulphur speciation, which, in turn is controlled by oxygen fugacity. Whilst sulphide has negligible solubility, sulphate ($[SO_4]^{2-}$) has a high solubility. It is, therefore, conceivable that an oxidising melt/fluid entered the diamond, through fractures, and oxidised and dissolved pre-existing sulphide as sulphate. After partial inclusion removal the "void" was then re-filled, predominantly by calcite. At the high pressures required for diamond stability, calcite is not a stable phase in peridotite as it would react with orthopyroxene to form magnesite and diopside. The epigenetic calcite inclusions, therefore, likely precipitated during kimberlite ascent.

Evidence for the involvement of alkali rich melts in the alteration of inclusions is derived from the observation of djerfisherite. In mantle xenoliths (e.g. Clarke et al., 1977, 1994; Henderson et al., 1999; Sharygin et al., 2007; Takechi et al., 2000) and as rare inclusions in diamonds (Bulanova et al., 1980), djerfisherite is believed to be the product of reactions between evolved kimberlitic melts/fluids, rich in K and Cl, and primary sulphides (typically pyrrhotite) (e.g. Bulanova et al., 1980; Sharygin et al., 2007). Supporting evidence for infiltration of diamond by an evolved, K rich melt/fluid comes from the presence of other epigenetic inclusions, including phlogopite and apatite.

7. Conclusions

Syngenetic inclusions in 33 diamonds from Renard indicate a predominantly peridotitic assemblage, typical for many diamond suites worldwide (worldwide the ratio: Peridotitic to eclogitic diamonds is 2:1; Stachel and Harris, 2008). Only one diamond contains likely eclogitic inclusions in the form of two low Ni sulphides. All silicate and oxide inclusions in the Renard suite are highly magnesian and garnets and Mg-chromites are very Cr rich. The average olivine Mg# (92.7) is similar to that observed from worldwide cratonic peridotites and closely corresponds to the experimentally determined point at which orthopyroxene is exhausted during partial melting. This suggests that Renard diamond sources likely originated during high-degrees of melt extraction (≥40%), initially leaving a dunitic residue behind. The high Cr# of the garnet and chromite inclusions implies that melt extraction, at least partially, occurred in the spinel stability field. As such, the Superior craton seems to have been built in a similar way to cratonic regions worldwide.

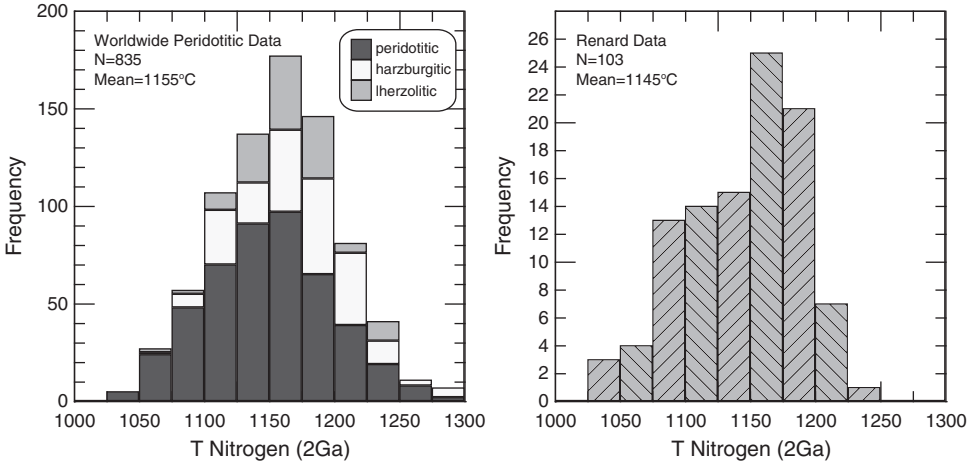

Fig. 9. Histogram of time averaged mantle residence temperatures separated into pipe number compared to worldwide lherzolitic, harzburgitic and "unspecified" peridotitic data (database of Stachel and Harris, 2008).

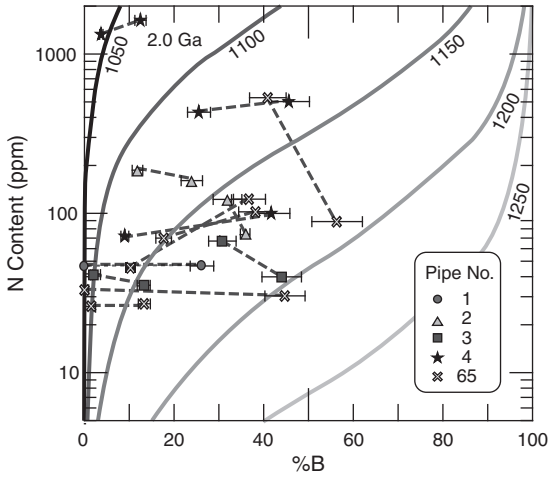

Fig. 10. Within diamond variations in nitrogen content and aggregation state that exceed analytical uncertainties (errors in N content determination are smaller than the symbol size and range between 10% (relative) below 500 ppm to 5% above 500 ppm; Precision for %B is ±5 (absolute)). Dashed tie lines connect analyses from single diamonds.

Abundant SiO_2 phase inclusions, confirmed to represent mainly coesite, are not interpreted to reflect eclogitic diamond sources. The presence of inclusions (high Mg# olivine and orthopyroxene) of indisputably peridotitic paragenesis together with coesite within the single diamonds clearly suggest that free SiO_2 formed during progressive carbonation reactions in peridotitic sources. The presence of SiO_2 inclusions together with olivine and orthopyroxene in four diamonds indicates that source carbonation occurred concurrent with diamond growth, with coesite precipitation representing the final stage of a series of carbonation reactions. Further evidence for an evolving diamond growth environment is derived from olivine inclusion with forsterite contents that vary up to ~0.5 for multiple inclusions in single diamonds.

The Renard diamonds have a narrow range in $\delta^{13}C$ from −5.4 to −1.2‰, with all but four of the diamonds having isotopic compositions between −4.6‰ and −2.6‰. The narrow range suggests an excess of diamond forming melts/fluids to suppress significant carbon isotopic fractionation effects. A similar mode, shifted slightly towards ^{13}C enriched isotopic compositions relative to the typical mantle value, was previously observed on the Superior Craton for a largely harzburgitic diamond suite from the Crystal showing at Wawa. Despite this slight shift to elevated $\delta^{13}C$ values, the carbon isotopic distribution is consistent with the observed predominantly peridotitic inclusion suite at Renard. Nitrogen based time averaged mantle residence temperatures (calculated for 2 Ga mantle residence) for the majority of diamonds fall between 1100 and 1200 °C, agreeing well with mineral inclusion based thermometry (1110–1180 °C). Consistency between these two different geothermometric approaches indicates that the residence time chosen for $T_{Nitrogen}$ is broadly realistic and that Renard diamonds, therefore, likely are Archean to Paleoproterozoic in age. Indications for multiple growth stages are observed for individual diamonds in the form of variations in nitrogen aggregation state at fairly constant nitrogen contents. This suggests successive diamond growth events over an extended time period (billions of years) or during relaxation back to a local geotherm following a thermal perturbation.

Supplementary data associated with this article can be found, in the online version, at doi:10.1016/j.lithos.2012.02.022.

Acknowledgements

The authors would like to thank Sergei Matveev for all his help with the electron microprobe. L.H. would like to acknowledge support from Alberta Innovates. T.S. acknowledges funding through an NSERC Discovery Grant and the Canada Research Chairs programme. We thank Andrew Kerr (Editor-in-chief) and K.S. Viljoen and an anonymous reviewer for their helpful reviews and constructive comments.

References

Armstrong, K.A., Nowicki, T.E., Read, G.H., 2004. Kimberlite AT-56: a mantle sample from the north central Superior craton, Canada. Lithos 77 (1–4), 695–704.
Ballhaus, C., Frost, B.R., 1994. The generation of oxidized CO_2-bearing basaltic melts from reduced CH4-bearing upper mantle sources. Geochimica et Cosmochimica Acta 58, 4931–4940.
Bernstein, S., Kelemen, P.B., Brooks, C.K., 1998. Depleted spinel harzburgite xenoliths in Tertiary dykes from East Greenland: Restites from high degree melting. Earth and Planetary Science Letters 154, 221–235.
Bernstein, S., Hanghøj, K., Kelemen, P.B., Brooks, C.K., 2006. Ultradepleted, shallow cratonic mantle beneath West Greenland: Dunitic xenoliths from Ubekendt Ejland. Contributions to Mineralogy and Petrology 152, 335–347.
Bernstein, S., Kelemen, P.B., Hanghøj, K., 2007. Consistent olivine Mg# in cratonic mantle reflects Archean mantle melting to the exhaustion of orthopyroxene. Geology 35 (5), 459–462.
Birch, F., Schairer, J.F., Spicer, H.C. (Eds.), 1942. Handbook of physical constants. Geological Society of America Special Papers Number 36. The Geological Society of America, Baltimore. 325 pp.
Birkett, T.C., McCandless, T.E., Hood, C.T., 2004. Petrology of the Renard igneous bodies: host rocks for diamond in the northern Otish Mountains region, Quebec. Lithos 76 (1–4), 475–490.
Bizzarro, M., Stevenson, R.K., 2003. Major element composition of the lithospheric mantle under the North Atlantic craton: evidence from peridotite xenoliths of the Sarfartoq area, southwestern Greenland. Contributions to Mineralogy and Petrology 146, 223–240.
Boyd, S.R., Kiflawi, I., Woods, G.S., 1994. The relationship between infrared-absorption and the a defect concentration in diamond. Philosophical Magazine B Physics of Condensed Matter Statistical Mechanics Electronic Optical and Magnetic Properties 69 (6), 1149–1153.
Boyd, S.R., Kiflawi, I., Woods, G.S., 1995. Infrared-absorption by the B-nitrogen aggregate in diamond. Philosophical Magazine B Physics of Condensed Matter Statistical Mechanics Electronic Optical and Magnetic Properties 72 (3), 351–361.
Boyd, R., Pokhilenko, N.P., Pearson, D.G., Mertzman, S.A., Sobolev, N.V., Finger, L.W., 1997. Composition of the Siberian cratonic mantle: evidence from Udachnaya peridotite xenoliths. Contributions to Mineralogy and Petrology 128, 228–246.
Brey, G.P., Köhler, T., 1990. Geothermobarometry in four-phase lherzolites: II. New thermobarometers, and practical assessment of existing thermobarometers. Journal of Petrology 31, 1353–1378.
Bulanova, G.P., Shestakova, O.E., Leskova, N.V., 1980. Djerfisherite from sulfide inclusions in diamonds. Doklady Akademii Nauk SSSR 255 (2), 430–433.
Bulanova, G.P., Griffin, W.L., Ryan, C.G., Shestakova, O.Y., Barnes, S.J., 1996. Trace elements in sulphide inclusions from Yakutian diamonds. Contributions to Mineralogy and Petrology 124, 111–125.
Bulatov, V., Brey, G.P., Foley, S.F., 1991. Origin of low-Ca, high-Cr garnets by recrystallization of low-pressure harzburgites. Fifth International Kimberlite Conference, Extended Abstracts: CPRM Spec Publ, 2/91, pp. 29–31.
Canil, D., Wei, K., 1992. Constraints on the origin of mantle-derived low Ca garnets. Contributions to Mineralogy and Petrology 109 (4), 421–430.
Cartigny, P., 2005. Stable isotopes and the origin of diamond. Elements 1 (2), 79–84.
Chacko, T., Mayeda, T.K., Clayton, R.N., Goldsmith, J.R., 1991. Oxygen and carbon isotope fractionations between CO_2 and calcite. Geochimica et Cosmochimica Acta 55 (10), 2867–2882.
Clark, S.P. (Ed.), 1966. Handbook of Physical Constants, Revised Edition. The Geological Society of America, Inc. Memoir, 97. The Geological Society of America, New York. 587 pp.
Clarke, D.B., Pe, G.G., MacKay, R.M., Gill, K.R., O'Hara, M.J., Gard, J.A., 1977. A new potassium–nickel sulfide from a nodule in kimberlite. Earth and Planetary Science Letters 35, 421–428.
Clarke, D.B., Mitchell, R.H., Chapman, C.A.T., MacKay, R.M., 1994. Occurrence and origin of Djerfisherite from the Elwin Bay kimberlite, Somerset Island, Northwest Territories. The Canadian Mineralogist 32, 815–823.
Collins, A.T., 1982. Colour centres in diamond. Journal of Gemmology 18, 37–75.
Coplen, T.B., Kendall, C., Hopple, J., 1983. Comparison of stable isotope reference samples. Nature 302 (5905), 236–238.
Davies, G., 1976. The A Nitrogen Aggregate in Diamond - Its Symmetry and Possible Structure. Journal of Physics C: Solid State Physics 9 (19), L537–L542.
Davies, R.M., Griffin, W.L., O'Reilly, S.Y., Andrew, A.S., 2003. Unusual mineral inclusions and carbon isotopes of alluvial diamonds from Bingara, eastern Australia. Lithos 69 (1–2), 51–66.
Dawson, J.B., Smith, J.V., Steele, I.M., 1992. 1966 ash eruption of Oldoinyo Lengai: mineralogy of lapilli, and mixing of silicate and carbonate magmas. Mineralogical Magazine 56, 1–16.
Dawson, J.B., Smith, J.V., Steele, I.M., 1995. Petrology and mineral chemistry of plutonic igneous xenoliths from the carbonatite volcano, Oldoinyo Lengai, Tanzania. Journal of Petrology 36, 797–826.
De Stefano, A., Kopylova, M.G., Cartigny, P., Afanasiev, V., 2009. Diamonds and eclogites of the Jericho kimberlite (Northern Canada). Contributions to Mineralogy and Petrology 158 (3), 295–315.

Deines, P., Harris, J.W., Spear, P.M., Gurney, J.J., 1989. Nitrogen and ^{13}C content of Finsch and Premier diamonds and their implications. Geochimica et Cosmochimica Acta 53 (6), 1367–1378.
Eggler, D.H., Baker, D.R., 1982. Reduced volatiles in the system C–O–H: implications for mantle melting, fluid formation and diamond genesis. In: Akimoto, S., Manghnani, M.H. (Eds.), High pressure research in geophysics. Center for Academic Publishing, Tokyo, pp. 237–250.
Evans, T., Harris, J.W., 1989. Nitrogen aggregation, inclusion equilibration temperatures and the age of diamonds. In: Ross, J., Jaques, A.L., Ferguson, J., Green, D.H., O'Reilly, S.Y., Danchin, R.V., Janse, A.J.A. (Eds.), Kimberlites and related rocks. Geological Society of Australia Special Publication no. 14, vol. 2. Blackwell Scientific Publications, Melbourne, pp. 1001–1006.
Evans, T., Qi, Z., Maguire, J., 1981. The stages of nitrogen aggregation in diamond. Journal of Physics C Solid State Physics 14 (12), L379–L384.
Fitzgerald, C.E., Hetman, C.M., Lepine, I.M., Skelton, D.S., McCandless, T.E., 2008. The internal geology and emplacement history of the Renard 2 kimberlite, Superior Province, Canada. Extended Abstract - 9th International Kimberlite Conference, Frankfurt, 2008.
Gaul, O.F., Griffin, W.L., O'Reilly, S.Y., Pearson, N.J., 2000. Mapping olivine composition in the lithospheric mantle. Earth and Planetary Science Letters 182 (3–4), 223–235.
Griffin, W.L., Shee, S.R., Ryan, C.G., Win, T.T., Wyatt, B.A., 1999. Harzburgite to lherzolite and back again: metasomatic processes in ultramafic xenoliths from the Wesselton kimberlite, Kimberley, South Africa. Contributions to Mineralogy and Petrology 134 (2–3), 232–250.
Griffin, W.L., O'Reilly, S.Y., Doyle, B.J., Pearson, N.J., Coopersmith, H., Kivi, K., Malkovets, V., Pokhilenko, N., 2004. Lithosphere mapping beneath the north American plate. Lithos 77 (1–4), 873–922.
Grütter, H.S., Gurney, J.J., Menzies, A.H., Winter, F., 2004. An updated classification scheme for mantle-derived garnet, for use by diamond explorers. Lithos 77 (1–4), 841–857.
Gurney, J.J., 1984. A correlation between garnets and diamonds in kimberlite. In: Harris, P.G., Glover, J.E. (Eds.), Kimberlite Occurrence and Origin: A Basis for Conceptual Models in Exploration. Geology Department and University Extensions, University of Western Australia, Perth, Western Australia, pp. 143–146. Special Publication 8.
Harris, J.W., 1968. Recognition of Diamond Inclusions .1. Syngenetic Mineral Inclusions. Industrial Diamond Review 28 (334), 402–410.
Harris, J.W., 1987. Recent physical, chemical, and isotopic research of diamonds. In: Nixon, P.H. (Ed.), Mantle Xenoliths. John Wiley and Sons.
Harris, J.W., 1992. Diamond geology. In: Field, J.E. (Ed.), The properties of diamond. Academic Press, London, pp. 345–393.
Harte, B., Fitzsimmons, I.C.W., Harris, J.W., Otter, M.L., 1999. Carbon isotope ratios and nitrogen abundances in relation to cathodoluminescence characteristics for some diamonds from the Kaapvaal Province, South Africa. Mineralogical Magazine 63, 829–856.
Henderson, C.M.B., Kogarko, L.N., Plant, D.A., 1999. Extreme closed system fractionation of volatile-rich, ultrabasic peralkaline melt inclusions and the occurrence of djerfisherite in the Kugda alkaline complex, Siberia. Mineralogical Magazine 63, 488–495.
Hunt, L., 2011. Conditions of diamond formation and preservation from on- and off-craton settings. Ph.D. Thesis. University of Alberta, Canada. http://hdl.handle.net.login.ezproxy.library.ualberta.ca/10048/2028.
Jaques, A.L., Hall, A.E., Sheraton, J.W., Smith, C.B., Sun, S.-S., Drew, R.M., Foudoulis, C., Ellingsen, K., 1989. Composition of crystalline inclusions and C-isotopic composition of Argyle and Ellendale diamonds. In: Ross, J., et al. (Ed.), Kimberlites and Related Rocks. Geological Society of Australia, Special Publication 14, vol. 2., Blackwell, Carlton, pp. 966–989.
Jugo, P.J., Luth, R.W., Richards, J.P., 2005. Experimental data on the speciation of sulfur as a function of oxygen fugacity in basaltic melts. Geochimica et Cosmochimica Acta 69 (2), 497–503.
Kaminsky, F.V., Zakharchenko, F.V., Griffin, W.L., Channer, D.M.D., Khachatryan-Blinova, G.K., 2000. Diamond from the Guaniamo area, Venezuela. The Canadian Mineralogist 38, 1347–1370.
Kelemen, P.B., Hart, S.R., Bernstein, S., 1998. Silica enrichment in the continental upper mantle via melt/rock reaction. Earth and Planetary Science Letters 164 (1–2), 387–406.
Kopylova, M.G., Russell, J.K., 2000. Chemical stratification of cratonic lithosphere: constraints from the northern Slave craton, Canada. Earth and Planetary Science Letters 181, 71–87.
Kopylova, M.G., Gurney, J.J., Daniels, L.R.M., 1997. Mineral inclusions in diamonds from the River Ranch kimberlite, Zimbabwe. Contributions to Mineralogy and Petrology 129 (4), 366–384.
Kullerud, G., Yund, R.A., Moh, G.H., 1969. Phase relations in the Cu-Fe-S, Cu-Ni-S and Fe-Ni-S systems. In: Wilson, H.D.B. (Ed.), Magmatic ore deposits. Economic Geology Publishing Co., Lancaster, pp. 323–343.
Leahy, K., Taylor, W.R., 1997. The influence of the Glennie domain deep structure on the diamonds in Saskatchewan kimberlites. Geologiya i Geofizika 38 (2), 451–460.
Lee, C.-T., Rudnick, R.L., 1999. Compositionally stratified cratonic lithosphere: petrology and geochemistry of peridotite xenoliths from the Labait tuff cone, Tanzania. In: Gurney, J.J., Gruney, J.L., Pascoe, M.D., Richardson, S.H. (Eds.), The Nixon volume, Proceedings of the 7th International Kimberlite Conference, pp. 503–521.
Leung, I.S., 1984. The discovery of calcite inclusion in natural diamond and its implications on the genesis of diamond, kimberlite and carbonatite. Geological Society of America, Abstracts with Programs 16, 574.
Litvin, Y.A., Butvina, V.G., 2004. Diamond-forming media in the system eclogite-carbonatite-sulfide-carbon: Experiments at 6.0–8.5 GPa. Petrology 12 (4), 377–387.
Litvin, Y.A., Shushkanova, A.V., Zharikov, V.A., 2005. Immiscibility of sulfide-silicate melts in the mantle: Role in the syngenesis of diamond and inclusions (based on experiments at 7.0 GPa). Doklady Earth Sciences 403 (5), 719–722.
Luth, R.W., 1993. Diamonds, eclogites, and the oxidation-state of the Earth's mantle. Science 261 (5117), 66–68.
Meyer, H.O.A., McCallum, M.E., 1986. Mineral inclusions in diamonds from the Sloan kimberlites, Colorado. Journal of Geology 94, 600–612.
Meyer, H.O.A., Milledge, H.J., Nave, E., 1965. Natural irradiation damage in Ivory Coast diamonds. Nature 206 (4982), 392.
Mitchell, R.H., 1997. Carbonate–carbonate immiscibility, neighborite and potassium iron sulphide in Oldoinyo Lengai natrocarbonatite. Mineralogical Magazine 61, 779–789.
Mitchell, R.H., Scott Smith, B.H., Larsen, L.M., 1999. Mineralogy of Ultramafic Dikes from the Sarfartoq, Sisimiut and Maniitsoq Areas, West Greenland. In: Gurney, J.J., Gurney, J.L., Pascoe, M.D., Richardson, S.H. (Eds.), Proceedings of the 7th International Kimberlite Conference, University of Cape Town, Cape Town, pp. 574–583.
O'Neill, H.S.C., Wood, B.J., 1979. An experimental study of the iron-magnesium partitioning between garnet and olivine and its calibration as a geothermometer. Contributions to Mineralogy and Petrology 70, 59–70.
Patterson, M., Francis, D., McCandless, T.E., 2009. Kimberlites: Magmas or mixtures? Lithos 112, 191–200.
Pearson, D.G., Canil, D., Shirey, S.B., 2003. 2.05 – mantle samples included in volcanic rocks: xenoliths and diamonds. In: Holland, H.D., Turekian, K.K. (Eds.), Treatise on Geochemistry. Pergamon, Oxford, pp. 171–275.
Percival, J.A., 2007. Geology and metallogeny of the Superior Province, Canada in, Mineral deposits of Canada: 471 a synthesis of major deposit-types, district metallogeny, the evolution of geological provinces, and exploration 472 methods. In: Goodfellow, W.D. (Ed.), Geological Association of Canada, Mineral Deposits Division, Special 473 Publication no. 5, pp. 903–928.
Phillips, D., Harris, J.W., 1995. Geothermobarometry of diamond inclusions from the De Beers Pool Mines, Kimberley, South Africa (abstract). 6th International Kimberlite Conference, Novosibirsk Extended Abstract, pp. 441–443.
Phillips, D., Harris, J.W., Viljoen, K.S., 2004. Mineral chemistry and thermobarometry of inclusions from De Beers Pool diamonds, Kimberley, South Africa. Lithos 77 (1–4), 155–179.
Polyakov, V.B., Kharlashina, N.N., 1995. The use of heat-capacity data to calculate carbon-isotope fractionation between graphite, diamond, and carbon-dioxide – a new approach. Geochimica et Cosmochimica Acta 59 (12), 2561–2572.
Richet, P., Bottinga, Y., Javoy, M., 1977. Review of hydrogen, carbon, nitrogen, oxygen, sulfur, and chlorine stable isotope fractionation among gaseous molecules. Annual Review of Earth and Planetary Sciences 5, 65–110.
Robinson, D.N., 1979. Surface textures and other features of diamonds. Ph.D. thesis, University of Cape Town, South Africa.
Rudnick, R.L., McDonough, W.F., Orpin, A., 1994. Northern Tanzanian peridotite xenoliths: A comparison with Kaapvaal peridotites and inferences on metasomatic interactions. In: Meyer, H.O.A., Leonardos, O. (Eds.), Kimberlites, related rocks and mantle xenoliths: Brasilia, Brazil, Companhia de Pesquisa de Recursos Minerai, vol. 1, pp. 336–353.
Sage, R.P., Lightfoot, P.C., Doherty, W., 1996. Bimodal cyclical Archean basalts and rhyolites from the Michipicoten (Wawa) greenstone belt, Ontario: geochemical evidence for magma contributions from the asthenospheric mantle and ancient continental lithosphere near the southern margin of the Superior Province. Precambrian Research 76 (3–4), 119–153.
Schidlowski, M., Hayes, J.M., Kaplan, I.R., 1983. Isotopic inferences of ancient biochemitries; carbon, sulfur, hydrogen, and nitrogen. In: Schopf, J.W. (Ed.), Earth's earliest biosphere; its origin and evolution. Princeton University Press, Princeton, NJ, pp. 149–186.
Schrauder, M., Navon, O., 1993. Solid carbon-dioxide in a natural diamond. Nature 365 (6441), 42–44.
Schulze, D.J., Harte, B., Valley, J.W., Brenan, J.M., Channer, D.M.D.R., 2003. Extreme crustal oxygen isotope signatures preserved in coesite in diamond. Nature 423 (6935), 68–70.
Scully, K.R., 2000. Kimberlites of the Attawapiskat area, James Bay Lowlands. Ontario Geological Survey, Northern Ontario.
Scully, K.R., Canil, D., Schulze, D.J., 2004. The lithospheric mantle of the Archean Superior Province as imaged by garnet xenocryst geochemistry. Chemical Geology 207 (3–4), 189–221.
Sellschop, J.P.F., Madiba, C.C.P., Annegarn, H.J., Shongwe, S., 1979. Volatile light elements in diamond. Diamond Research, Industrial Diamond Information Bureau, London, United Kingdom, pp. 24–30.
Sharygin, V.V., Golovin, A.V., Pokhilenko, N.P., Kamenetsky, V.S., 2007. Djerfisherite in the Udachnaya-East pipe kimberlites (Sakha-Yakutia, Russia): paragenesis, composition and origin. European Journal of Mineralogy 19 (1), 51–63.
Shushkanova, A.V., Litvin, Y.A., 2005. Phase relations in diamond-forming carbonate-silicate-sulfide systems on melting. Russian Geology and Geophysics 46 (12), 1317–1326.
Shushkanova, A.V., Litvin, Y.A., 2008. Diamond formation in sulfide pyrrhotite-carbon melts: Experiments at 6.0-7.1 GPa and application to natural conditions. Geochemistry International 46 (1), 37–47.
Sobolev, N.V., Yefimova, E.S., Channer, D.M.D., Anderson, P.F.N., Barron, K.M., 1998. Unusual upper mantle beneath Guaniamo, Guyana shield, Venezuela: evidence from diamond inclusions. Geology 26 (11), 971–974.
Sobolev, N.V., Logvinova, A.M., Zedgenizov, D.A., Seryotkin, Y.V., Yefimova, E.S., Floss, C., Taylor, L.A., 2004. Mineral inclusions in microdiamonds and macrodiamonds from kimberlites of Yakutia: a comparative study. Lithos 77 (1–4), 225–242.
Sobolev, N.V., Logvinova, A.M., Efimova, E.S., 2009. Syngenetic phlogopite inclusions in kimberlite-hosted diamonds: implications for role of volatiles in diamond formation. Russian Journal of Geology and Geophysics 50, 1234–1248.

Stachel, T., 2007. Diamond. Mineralogical Association of Canada Short Course Series, 37, pp. 1–22.
Stachel, T., Harris, J.W., 2008. The origin of cratonic diamonds – constraints from mineral inclusions. Ore Geology Reviews 34, 5–32.
Stachel, T., Harris, J.W., Brey, G.P., 1998a. Rare and unusual mineral inclusions in diamonds from Mwadui, Tanzania. Contributions to Mineralogy and Petrology 132 (1), 34–47.
Stachel, T., Viljoen, K.S., Brey, G., Harris, J.W., 1998b. Metasomatic processes in lherzolitic and harzburgitic domains of diamondiferous lithospheric mantle: REE in garnets from xenoliths and inclusions in diamonds. Earth and Planetary Science Letters 159 (1–2), 1–12.
Stachel, T., Harris, J.W., Brey, G.P., Joswig, W., 2000. Kankan diamonds (Guinea) II: lower mantle inclusion parageneses. Contributions to Mineralogy and Petrology 140, 16–27.
Stachel, T., Harris, J.W., Tappert, R., Brey, G.P., 2003. Peridotitic diamonds from the Slave and the Kaapvaal cratons – similarities and differences based on a preliminary data set. Lithos 71 (2–4), 489–503.
Stachel, T., Banas, A., Muehlenbachs, K., Kurszlaukis, S., Walker, E.C., 2006. Archean diamonds from Wawa (Canada): samples from deep cratonic roots predating cratonization of the Superior Province. Contributions to Mineralogy and Petrology 151 (6), 737–750.
Stachel, T., Harris, J.W., Muehlenbachs, K., 2009. Sources of carbon in inclusion bearing diamonds. Lithos 112, 625–637.
Takechi, Y., Kusachi, I., Nakamuta, Y., Kase, K., 2000. Nickel-bearing djerfisherite in gehlenite-spurrite skarn at Kushiro, Hiroshima Prefecture, Japan. Resource Geology 50, 179–184.
Taylor, W.R., 1988. Measurement of reduced peridotite-C-O-H solidus and implications for redox melting of the mantle. Nature 332 (6162), 349–352.
Taylor, L.A., Liu, Y., 2009. Sulfide inclusions in diamonds: not monosulfide solid solution. Russian Geology and Geophysics 50 (12), 1201–1211.
Taylor, W.R., Jaques, A.L., Ridd, M., 1990. Nitrogen-defect aggregation characteristics of some Australasian diamonds; time–temperature constraints on the source regions of pipe and alluvial diamonds. American Mineralogist 75 (11–12), 1290–1310.
Taylor, W.R., Canil, D., Milledge, H.J., 1996. Kinetics of Ib to IaA nitrogen aggregation in diamond. Geochimica et Cosmochimica Acta 60 (23), 4725–4733.
Van Rythoven, A.D., McCandless, T.E., Schulze, D.J., Bellis, A., Taylor, L.A., Liu, Y., 2011. Diamond crystals and their mineral inclusions from the Lynx Kimberlite Dyke Complex, Central Quebec. The Canadian Mineralogist 49, 691–706.
Von Seckendorff, V., O'Neill, H.S.C., 1993. An experimental study of Fe-Mg partition between olivine and orthopyroxene at 1173, 1273 and 1423 K and 1.6 GPa. Contributions to Mineralogy and Petrology 113, 196–207.
Walter, M.J., 1999. Melting residues of fertile peridotite and the origin of cratonic lithosphere. In: Fei, Y., Bertka, C.M., Mysen, B.O. (Eds.), Mantle petrology: field observations and high pressure experimentation: A tribute to Francis R. (Joe) Boyd. Special Publication. The Geochemical Society, Houston, pp. 225–239.
Wang, A., Pasteris, J.D., Meyer, H.O.A., DeleDuboi, M.L., 1996. Magnesite-bearing inclusion assemblage in natural diamond. Earth and Planetary Science Letters 141 (1–4), 293–306.
Woods, G.S., 1986. Platelets and the Infrared-Absorption of Type-Ia Diamonds. Proceedings of the Royal Society A Mathematical, Physical and Engineering Sciences 407 (1832), 219–238.
Wyllie, P.J., 1978. Mantle fluid compositions buffered in peridotite-CO_2-H_2O by carbonates, amphibole: and phlogopite. Journal of Geology 86, 687–713.
Wyllie, P.J., Huang, W.L., 1976. Carbonation and melting reactions in system Cao-MgO-SiO_2-CO_2 at mantle pressures with geophysical and petrological applications. Contributions to Mineralogy and Petrology 54 (2), 79–107.
Wyllie, P.J., Huang, W.L., Otto, J., Byrnes, A.P., 1983. Carbonation of peridotites and decarbonation of siliceous dolomites represented in the system CaO-MgO-SiO_2-CO_2 to 30 kbar. Tectonophysics 100, 359–388.
Yavuz, F., 2007. WinAmphcal: A Windows program for the IMA-04 amphibole classification. Geochemistry, Geophysics, Geosystems 8 (1), Q01004.
Yefimova, E.S., Sobolev, N.V., Pospelova, L.N., 1983. Sulfide inclusions in diamond and specific features of their paragenesis. Zapiski Vsesoyuznogo Mineralogicheskogo Obshchestva 112 (3), 300–310.

Web reference

Handbook of Minerals Raman Spectra. Free database 2000-2012 Laboratoire de Sciences de la Terre ENS-Lyon France. http://www.ens-lyon.fr/LST/Raman/. 28/12/2011.